

The Sundowner Winds Experiment (SWEX) in Santa Barbara, California

Advancing Understanding and Predictability of Downslope Windstorms in Coastal Environments

Leila M. V. Carvalho , Gert-Jan Duine, Craig Clements, Stephan F. J. De Wekker, Harindra J. S. Fernando, David R. Fitzjarrald, Robert G. Fovell, Charles Jones, Zhien Wang, Loren White, Anthony Bucholtz, Matthew J. Brewer, William Brown, Matt Burkhart, Edward Creegan, Min Deng, Marian de Orla-Barile, David Emmitt, Steve Greco, Terry Hock, James Kasic, Kiera Malarkey, Griffin Modjeski, Steven Oncley, Alison Rockwell, Daisuke Seto, Callum Thompson, and Holger Vömel

KEYWORDS:

Downslope winds;
Boundary layer;
Lidar observations;
Mountain
meteorology;
Mesoscale
processes; Profilers,
atmospheric

ABSTRACT: Coastal Santa Barbara is among the most exposed communities to wildfire hazards in Southern California. Downslope, dry, and gusty windstorms are frequently observed on the south-facing slopes of the Santa Ynez Mountains that separate the Pacific Ocean from the Santa Ynez valley. These winds, known as “Sundowners,” peak after sunset and are strong throughout the night and early morning. The Sundowner Winds Experiment (SWEX) was a field campaign funded by the National Science Foundation that took place in Santa Barbara, California, between 1 April and 15 May 2022. It was a collaborative effort of 10 institutions to advance understanding and predictability of Sundowners, while providing rich datasets for developing new theories of downslope windstorms in coastal environments with similar geographic and climatic characteristics. Sundowner spatiotemporal characteristics are controlled by complex interactions among atmospheric processes occurring upstream (Santa Ynez valley), and downstream due to the influence of a cool and stable marine boundary layer. SWEX was designed to enhance spatial measurements to resolve local circulations and vertical structure from the surface to the midtroposphere and from the Santa Barbara Channel to the Santa Ynez valley. This article discusses how SWEX brought cutting-edge science and the strengths of multiple ground-based and mobile instrument platforms to bear on this important problem. Among them are flux towers, mobile and stationary lidars, wind profilers, ceilometers, radiosondes, and an aircraft equipped with three lidars and a dropsonde system. The unique features observed during SWEX using this network of sophisticated instruments are discussed here.

<https://doi.org/10.1175/BAMS-D-22-0171.1>

Corresponding author: Leila M. V. Carvalho, leila@eri.ucsb.edu

In final form 21 November 2023

© 2024 American Meteorological Society. This published article is licensed under the terms of the default AMS reuse license. For information regarding reuse of this content and general copyright information, consult the AMS Copyright Policy (www.ametsoc.org/PUBSReuseLicenses).

AFFILIATIONS: Carvalho, Duine, Jones, de Orla-Barile, Seto, and Thompson—University of California, Santa Barbara, Santa Barbara, California; Clements and Malarkey—San Jose State University, San Jose, California; De Wekker—University of Virginia, Charlottesville, Virginia; Fernando, Creegan, and Modjeski—University of Notre Dame, South Bend, Indiana; Fitzjarrald, Fovell, and Brewer—University at Albany, State University of New York, Albany, New York; Wang—Stony Brook University, State University of New York, Stony Brook, New York; Kasic—University of Colorado Boulder, Boulder, Colorado; White—Jackson State University, Jackson, Mississippi; Bucholtz—Naval Postgraduate School, Monterey, California; Brown, Hock, Oncley, Rockwell, and Vömel—National Center for Atmospheric Research, Boulder, Colorado; Burkhardt—University of Wyoming, Laramie, Wyoming; Deng—Brookhaven National Laboratory, Upton, New York; Emmitt—Simpson Weather Associates Inc., Charlottesville, Virginia; Greco—Army Research Laboratory, White Sands Missile Range, New Mexico

Wildfires are among the greatest natural hazards in the western United States and other parts of the world. Coastal Santa Barbara (SB), with nearly 160,000 inhabitants, is particularly exposed to wildfires, as communities live in a narrow zone between the east–west-oriented Santa Ynez Mountains (SYM) and the SB Channel (Fig. 1). Gusty, downslope winds, known as Sundowner winds (or Sundowners) are frequently observed on the southern slopes of the SYM. These are episodes of northerly (cross-mountain) gusty winds that typically peak after sunset (the reason for the name) and often remain strong from night to early morning hours. Intriguingly, Sundowners exhibit a remarkable spatial and temporal variability along the southern slopes of the SYM (Blier 1998; Cannon et al. 2017; Smith et al. 2018; Carvalho et al. 2020; Jones et al. 2021; Zigner et al. 2021; Duine et al. 2019, 2021, 2022). These gusty winds are often accompanied by mountain waves and wave breaking (Carvalho et al. 2020; Duine et al. 2019), wave-induced critical layers (Cannon et al. 2017), rapid decreases in dewpoint and relative humidity, and local changes in nighttime cooling rate. Sundowners have enhanced numerous fast-spreading wildfires that disrupted local communities (Zigner et al. 2020, 2022), leading to massive evacuations, property and life losses, and significant environmental impacts.

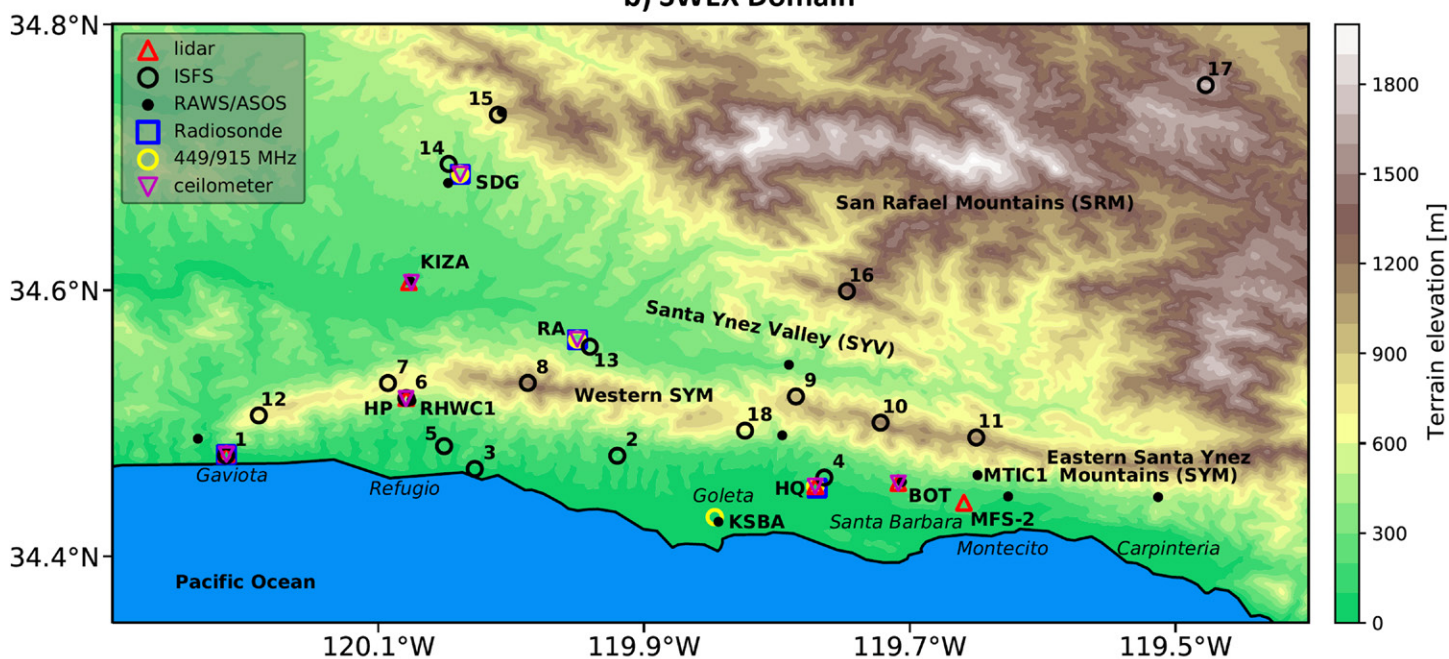
Sundowners can occur year-round, but the highest frequency of these events is observed from March to May (Hatchett et al. 2018; Jones et al. 2021). Three types of Sundowner regimes have been recognized (Jones et al. 2021): “western Sundowners,” characterized by winds from a northwest to north direction with the strongest winds typically between late afternoon and early evening on the western SYM (Gaviota and Refugio, Fig. 1); “eastern Sundowners,” characterized by winds from a northeast to north direction with the strongest winds typically from late evening to early morning on the eastern slopes of the SYM (Santa Barbara and Montecito, Fig. 1). These two regimes may occur independently or together (hybrid events). When hybrid, strong winds are generally observed over both the eastern and western slopes of the SYM, with gusts peaking at different times of the evening (late afternoon to early evening over western and late evening to early morning over eastern SYM). This wind regime was named “Santa Barbara” in Jones et al. (2021).

The synoptic forcing of Sundowners is reasonably well understood. Jones et al. (2021) showed that western Sundowners are typically associated with a ridge over the Pacific, a trough over the western United States (“sliding low”), and cold temperature advection in the lower troposphere. Eastern Sundowners are related to the enhancement of a ridge over the

a) SWEX Instrument platforms



b) SWEX Domain



c) SWEX Flight Tracks

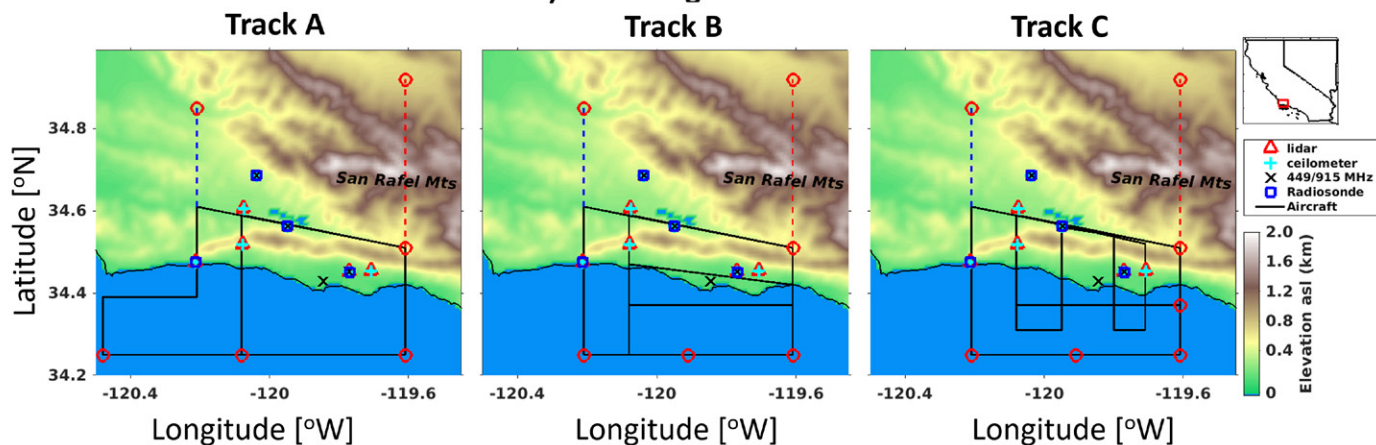


Fig. 1. (a) Example of instrument platforms deployed during the SWEX campaign. Facility provider and location are indicated in each frame; (b) SWEX domain, topography (colors), and instruments (symbols). Open black circles with numbers indicate NCAR ISFS flux towers. USFS RAWs and NWS stations are shown as dark dots (see appendix A for acronyms). Symbols for all other instruments are described in the figure's legend. BOT, HQ, HP, RA, and SDG have multiple instruments (see appendix B). MFS-2 lidar refers to IOP-10. (c) Twin-Otter flight tracks (lines) overlaying SWEX domain and orography. Dashed lines indicate afternoon initial dropsonde at Cuyama valley (red) and Sisquoc wilderness (blue) (see text for details). Flight legs followed the same direction (counterclockwise). Red circles indicate dropsondes sites. Target flight elevations at 3,352 m MSL were adopted for dropsondes and 2,438 m MSL to optimize lidar operations. The SWEX domain within the state of California is shown in the inset map.

Pacific, which extends over the West Coast of the United States. The hybrid regime results from a combination of both western and eastern regimes but with a stronger North Pacific subtropical high with spatial patterns that resample the eastern regime. However, mechanisms explaining the spatiotemporal variability, timing, and intensity of the strongest winds, temperature, and humidity profiles up- and downwind of the SYM are understudied.

Most of the Sundowner theory has heavily relied on simulations with regional models that have not been properly compared against observations. During a 2-day Sundowner pilot study (28–29 April 2018), 3-hourly radiosondes were launched downstream of the SYM revealing peculiar aspects of a western Sundowner event (Carvalho et al. 2020). For example, radiosondes indicated that the onset of Sundowners was associated with the enhancement of a lee-slope jet near ground level, an increase in stability in the ABL and the presence of mountain waves on the lee side of the SYM. Interestingly, winds did not remain strong throughout the evening. Rather, they weakened for a few hours to reintensify later in a very shallow layer above ground level. The weakening and reinvigoration of the lee-slope jet could not be explained by similar mechanisms and could not be properly forecasted, suggesting that unknown processes acting on meso- to turbulent scales are relevant to explain Sundowner behavior. Weather stations on the SYM slopes have shown that these “double” peaks in nighttime winds often occur during Sundowners.

Simulations with the Weather Research and Forecasting (WRF) Model (Skamarock et al. 2019) of this and other events have indicated that enhanced offshore winds induce horizontal wind shear over the SB channel that form mesoscale eddies. Those eddies may advect the marine ABL inland, playing a role in the spatiotemporal variability of surface winds. Therefore, in addition to mountain wave theory, Sundowner behavior may depend on complex interactions between the marine and continental ABLs. Understanding these mechanisms and assessing their potential predictability have critical impacts on fire weather forecast and cannot be done without adequate measurements.

The Sundowner Winds Experiment (SWEX) was designed to obtain strategic observations of ABL processes, mountain waves, and critical layers to advance the understanding and predictability of Sundowner winds, while providing rich datasets for the development of new theories of downslope windstorms in coastal environments. The campaign deployed sophisticated instrument platforms to enhance spatial measurements of atmospheric variables from the SB Channel to the Santa Ynez valley (Fig. 1). SWEX specifically addressed the following scientific objectives: 1) investigate how the structure and dynamics of marine and continental ABLs influence mountain flows during Sundowners and undisturbed periods, including intensity, timing, and geographic characteristics of the downslope winds; 2) examine mechanisms relating mountain waves, critical layers, and surface wind intensity leeward of the SYM; 3) investigate how variations in ABL structure and tropospheric stability control mountain wave-induced flow and the predictability of Sundowner winds.

SWEX extended from 1 April to 15 May 2022. It was the first field campaign in Southern California to investigate mechanisms driving downslope windstorms in a narrow coastal mountain range that is influenced by a cool and shallow stably stratified marine ABL (SSMBL). SWEX was a joint effort of 10 institutions (appendix B) and an opportunity for transferring the scientific findings of a field campaign to operational daily forecast needs of the National Weather Service Los Angeles/Oxnard (LOX) office.

The SWEX field campaign design

SWEX domain. The spatiotemporal variability of Sundowners is intrinsically related to the SB unique topography (Duine et al. 2021). The east–west-oriented SYM rise abruptly from the coast, with elevations increasing from west to east and peaks ranging between 600 and 1,200 m (Fig. 1). Upstream (i.e., north), the San Rafael Mountains (SRM),

with elevations exceeding 2,000 m, merge with the SYM on its eastern flank, creating the V-shaped Santa Ynez valley (SYV). Thus, the SYM act as a natural barrier between the humid and cool SSMBL on the south, which typically forms over the cool waters of the Pacific Ocean, and the much drier ABL that develops in the SYV. When synoptic conditions favor strong winds with northerly component (cross-mountain winds), these contrasting ABLs are instrumental in the spatiotemporal variability of Sundowners. SWEX was designed to obtain key meteorological observations to evaluate ABL evolution, winds, and thermodynamic structure of the lower troposphere upstream of the SYM (i.e., the SYV and SRM), at ridgeline, midslopes, and foothills of the SYM, and over the SB Channel (Fig. 1). The SWEX domain extended approximately 60 km in the east–west direction and 35 km in the north–south direction (Fig. 1) over historical indigenous land. It encompassed the cities of Goleta and Santa Barbara, and the communities of Gaviota, Refugio, and Montecito on the coast, as well as five towns (Ballard, Buellton, Los Olivos, Santa Ynez, and Solvang), several rural communities, ecological preserves, and the Chumash Reservation in the SYV.

Ground instruments. The experimental plan was designed to investigate micro- to meso-scale mechanisms associated with Sundowners, and how they contrast with undisturbed conditions. Ground-based instruments were placed at strategic locations (on both private and public land) to observe the evolution and characteristics of the ABL, particularly focusing on spatial gradients and temporal variability of winds, temperature, humidity, and pressure. These instruments collected observations from 1 April to 15 May 2022. The ground-based instrumental platforms consisted of surface flux towers (NCAR ISFS), radar wind profilers, Doppler lidars, ceilometers, infrasound sensors, microwave radiometers, and radiosondes (Fig. 1). All acronyms and abbreviations are summarized in appendix A. Instrument specification, location, and facility provider are shown in appendix B, Table B1.

Thirteen NCAR ISFS 10-m flux towers were distributed along the SYM ridgeline, south-facing slopes, and foothills of the SYM. Instruments were placed at strategic sites to examine the contrasting behavior between eastern and western Sundowners (Fig. 1). A stationary Doppler lidar and a ceilometer (both UND) surveilled the eastern portion of the SYM while two Doppler lidars (UND, SJSU) and two ceilometers (UND, UAlbany) were placed on the southern slopes of the western SYM. At the westernmost site of the SWEX domain, on the foothills of the SYM in Gaviota, a Doppler lidar (SJSU), ISFS tower, a radiosonde system (SJSU) and a small triangular array of infrasound sensors with a near-surface sonic anemometer (UAlbany) complemented these instruments. Furthermore, a 449-MHz radar wind profiler, a Doppler lidar, a ceilometer, and a meteorological tower (NCAR ISS) were installed on the southern foothills of the central-eastern SYM, near the site where radiosondes were launched during the SWEX pilot experiment (Carvalho et al. 2020). A radiosonde system (SJSU) complemented the set of instruments at that site.

To evaluate meteorological conditions upstream of the SYM, five NCAR ISFS 10-m flux towers were spatially distributed approximately along north–south transects, from the foothills of the SRM to the southern slopes of the SYM. These towers were placed at distinct elevations across the SYV and SRM (Fig. 1, Table B1). Two NCAR ISS 915-MHz radar wind profilers, two ceilometers, and one NCAR ISS RASS obtained high-resolution ABL winds profiles on the western SYV (UCSB Sedgwick Reserve) and eastern SYV (Rancho Alegre) (Fig. 1). Both sites included one NCAR ISS radiosonde system. A Doppler lidar, ceilometer, microwave radiometer, and meteorological tower (UND) complemented these measurements at the center of the SYV (at the Santa Ynez Airport), approximately aligned with the UND Doppler lidar placed on the southern slopes of the SYM in Refugio (Fig. 1). Except for the radiosonde systems, all other

ground instruments recorded measurements throughout the 45 days of the campaign, with a few exceptions (see appendix B).

Mobile instruments. The SWEX campaign explored novel methods to evaluate the spatial contrasts and temporal variability of winds, temperature, and humidity profiles within the ABL by integrating three complementary mobile platforms, one airborne and two ground-based.

The University of Virginia Wind Observatory on Wheels (UWOW) used a scanning Doppler lidar (Halo Photonics Streamline XR) installed in a 3.7-m cargo trailer to obtain vertical profiles of horizontal winds up to ~3,000 m AGL and with a horizontal spacing of ~1 km. UWOW collected data along north–south transects and east–west routes near the foothills (e.g., U.S. 101) several times during special operations. With this strategy, UWOW identified spatial contrasts in wind profiles within the ABL up- and downstream of the SYM, revealing remarkable spatial transitions in regime flow (e.g., from light winds to strong lee-slope jets) along the foothills of the SYM. Furthermore, its mobility allowed comparisons with multiple ground (e.g., ISS lidars) and airborne instrumentation. Between operations, UWOW was maintained stationary, continuously collecting wind profiles primarily at two sites, next to San Marcos Pass and next to the ISS lidar at the SBCFD-HQ. During IOP-10, UWOW was placed at the Montecito Fire Station-2 (MFS-2, Fig. 1), in Montecito.

The mobile meteorological unit JSU-MMU (White 2014; White and Lu 2020) collected near-ground observations of temperature and humidity at 2-s increments, incoming solar radiation, infrared brightness temperature (sky/cloud), and pressure. These instruments were mounted on a regular automobile with global positioning system (GPS). Measurements often followed similar tracks as for UWOW, and included east–west transects along the crest of the SYM (Camino Cielo Road) complementing the UWOW mobile observations. The JSU-MMU made it possible to identify contrasts in air masses and was particularly useful in characterizing transitions between the “warm and dry belt” associated with Sundowners and the “cool and moist” marine ABL at lower elevations.

The NPS/CIRPAS Twin-Otter airborne platform was critical in obtaining profiles of winds, humidity, temperature, and aerosol distribution at high spatial resolution over the SB Channel, across the SRM and SYM, and along the SYV. The airborne instrumentation provided unique ways to properly characterize mountain waves, document spatial gradients, and observe transition layers in the lower troposphere. These measurements complemented ground and mobile observations in remote regions with no other instrumental coverage. In addition to in situ measurements (3D wind and turbulence, temperature, water vapor, and static pressure), the Twin-Otter was equipped with three lidars. The compact rotational Raman lidar (CRL) (Liu et al. 2014; Wu et al. 2016) obtained 2D distributions of water vapor, aerosols, temperature, and cloud optical properties in the lower troposphere and ABL at a vertical resolution of about 50 m. The Twin-Otter Doppler Wind Lidar (TODWL) (De Wekker et al. 2012; Emmitt and Godwin 2014) performed downward conical scans with a laser beam, obtaining vertical profiles of horizontal and vertical winds at a vertical resolution of 50 m. The Wyoming Cloud Lidar (WCL) measured cloud base profiles, cloud and aerosol extinction coefficients, and provided depolarization profiles (Wang et al. 2009). The NCAR AVAPS dropsonde system (Vömel et al. 2021) complemented these measurements with vertical profiles of temperature, humidity and winds that were also useful for instrumental calibration. The Twin-Otter followed multiple transects that were planned according to the type of operation and forecast of wind patterns (Fig. 1).

Types of special operations and campaign strategy

Two types of special operations were conducted during SWEX (Table 1): intensive operation period (IOP) and enhanced operation period (EOP). IOPs were designed to obtain lower-troposphere measurements when synoptic conditions favored strong cross-mountain

Table 1. IOP and EOP date and time (starting time and ending time, UTC), Sundowner Regime, flight track A–C (Fig. 1), number of dropsondes in the afternoon and evening flights, and total number of radiosondes at SBCFD-HQ (HQ), SBCFD-38 (GVT), Sedgwick (SDG), and Rancho Alegre (RA). Distances driven by UWOW and JSU (km) are shown in the last two columns. TODWL refers to the Office of Naval Research (ONR)-sponsored augmentation hours aimed to intercompare airborne and ground-based wind profilers and lidars, investigate beam attenuation during strong coastal jets, and evaluate performance of the Doppler lidar in observing vertical velocity associated with mountain waves.

IOP/EOP	Time and date	Regime	Airplane track	Dropsonde (afternoon, evening)	Radiosonde (HQ, GVT, SDG, RA)	UWOW (km)	JSU (km)
IOP-1	1700 UTC 4 Apr 1400 UTC 5 Apr	Eastern	A	5, 8	7, 8, 8, 8	379	255
IOP-2	2300 UTC 5 Apr 0800 UTC 6 Apr	Eastern (hybrid)	A ^a (half day)	0, 9	4, 4, 1, 4	119	177
IOP-3	1700 UTC 13 Apr 1400 UTC 14 Apr	Western	A	5, 8	8, 8, 7, 8	672	209
IOP-4	1700 UTC 18 Apr 1400 UTC 19 Apr	Western	B	5, 9	6, 8, 8, 6	595	135
IOP-5	1700 UTC 23 Apr 1400 UTC 24 Apr	Eastern (hybrid)	B	7, 8	8, 8, 8, 8	708	383
IOP-6	1700 UTC 28 Apr 0800 UTC 29 Apr	Western	B	6, 8	8, 8, 8, 8	739	316
IOP-7 and TODWL	2300 UTC 7 May 0530 UTC 8 May	Western	(Half day)	7	3, 3, 3, 3	406	204
IOP-8	1700 UTC 8 May 1400 UTC 9 May	Western	C	7, 9	10, 10, 10, 10	600	374
IOP-9	1700 UTC 10 May 1400 UTC 11 May	Western	C	5, 10	9, 9, 9, 9	642	317
IOP-10	2300 UTC 12 May 1400 UTC 13 May	Eastern	No flights	0	4, ^b 0, 0, 7	Stationary	78
EOP-1	1700 UTC 17 Apr 1400 UTC 18 Apr	—	A	5, 8	8, 8, 8, 8	540	240
EOP-2	1700 UTC 25 Apr 1400 UTC 26 Apr	—	B	6, 9	8, 8, 7, 8	719	143
EOP-3	1700 UTC 4 May 1400 UTC 5 May	—	C	6, 9	10, 10, 10, 10	754	408

^a Shorter flight track (inner box, track A, Fig. 1).

^b Radiosondes released from Montecito Fire Department station-2 (MFS-2).

Sundowner winds (excluding frontal systems). Events representative of pre- and postfrontal systems, heatwaves, and conditions associated with weak upper-level winds were also of interest. IOPs were categorized according to the type of Sundowner wind regime: western, eastern, or hybrid. The definition of wind regimes was primarily important for planning mobile measurement strategies.

EOPs were designed to represent the undisturbed conditions along the southern SYM. During IOPs and EOPs, measurements were enhanced by 3-hourly radiosondes in two sites downstream of the SYM (Gaviota and HQ, Fig. 1) and two sites upstream in the SYV (SDG and RA, Fig. 1). Mobile measurements were conducted during all IOPs/EOPs, except for IOP-10 (Table 1).

IOPs and EOPs officially started at 1000 PDT (first radiosondes) on the day of the event and ended at 0700 PDT (last radiosondes) of the next day, with a few exceptions (see Table 1). The final decision on a mission was made 24 h in advance.

Event forecast. IOPs and EOPs were decided based on daily forecast discussions prepared by the National Weather Service, LA/Oxnard office (NWS/LOX) at 1000 PDT. The synoptic analyses focused on 5-day forecasts using the European Centre for Medium-Range Weather Forecasts (ECMWF) and the National Centers for Environmental Prediction Global Forecast System (GFS) models, complemented with 48 h (updated four times daily) forecasts with the High-Resolution Rapid Refresh (HRRR). The NWS/LOX has developed special metrics to identify synoptic conditions that are frequently associated with Sundowners. These include upper-level forcing, generally characterized by the proximity of the subtropical jet, forecast of cold advection, and strong mean sea level pressure (MSLP) gradients. Specifically, the NWS/LOX developed empirical indices that relate MSLP differences between the SB and Santa Maria airports (KSBA–KSMX) and SB and Bakersfield airports (KSBA–KBFL) to the strength of Sundowner winds (Ryan 1996).

Mesoscale features were evaluated using 84-h forecasts performed at UCSB with WRF at 2-km grid-spacing resolution, with configuration described in Jones et al. (2021) based on model sensitivity discussed in Duine et al. (2019). WRF initial and boundary conditions were provided by the NCEP North American Mesoscale Forecasting System (NAM).

SWEX extended over a period with numerous days with cross-mountain gusty winds. However, days representative of truly quiescent conditions were scarce, resulting in fewer opportunities to conduct EOPs than expected. SWEX had 13 missions: 10 were IOPs and 3 EOPs (Table 1).

Mission strategy, flight plans, and ground mobile operations. Each IOP/EOP consisted of a separate afternoon and evening flight that were planned 24 h in advance of each mission to maximize observations according to the forecasted wind behavior. Afternoon flights typically lasted around 3 h and were designed to capture the state of the atmosphere preceding the Sundowner onset. Evening flights typically lasted 4 h and were planned to observe atmospheric conditions approximately during and after the onset of the strongest downslope winds. Some flight tracks intersected ground profiler systems for comparison purposes (Fig. 1).

The initial dropsonde in the afternoon flight obtained conditions upstream of the study area, i.e., farther north of the SYM, and varied according to the forecast: over Cuyama valley (northeast of the domain, $\sim 34.92^{\circ}\text{N}$, 119.61°W) during eastern regimes, and over Sisquoc wilderness, Santa Maria County (northwest of the domain, 34.85°N , 120.21°W) during western regimes. When hybrid regimes were forecasted, the initial dropsonde was over Cuyama valley.

The multiple west–east flight tracks (Fig. 1, bottom) were designed to capture the evolution of the ABL depth and contrasts in temperature, winds, and humidity profiles along the SYV and over the ocean along the SB Channel. Mountain wave structure and associated profiles of aerosols, temperature, humidity, and winds were investigated with multiple north–south cross-mountain legs targeting three locations: Gaviota, Refugio, and Montecito (Fig. 1). However, flight tracks varied during the experiment. For instance, some (track A, Fig. 1) specifically targeted the evolution of the coastal jet (Rahn et al. 2013), conjectured to be associated with the development of western Sundowners (Smith et al. 2018; Jones et al. 2021; Zigner et al. 2021), whereas others focused on lee-side ABL characteristics along multiple east–west-oriented legs (track B, Fig. 1). Multiple cross-mountain flights (track C, Fig. 1) were explored in some IOPs to complement these observations. Exceptions were IOP-2, which focused solely on the eastern portions of the study area, IOP-7 that explored different tracks to obtain vertical and horizontal velocity profiles across the SYM and SRM, and IOP-10 with no flights.

Ground mobile measurements (UWOW and JSU-MMU) generally extended from midafternoon to early evening hours to properly characterize the diurnal evolution of the ABL preceding and after the expected onset of Sundowners. These mobile operations were optimized

according to the category of event, prioritizing the portion of the domain expected to observe the strongest winds during IOPs.

Radiosonde launches, flight tracks (including dropsonde locations), and ground mobile measurements during EOPs replicated IOPs. Since wind regimes were not defined in these cases, the first dropsonde during the afternoon flight was decided based on forecast of calm nighttime winds in Gaviota (western regime paths) or Montecito (eastern regime paths) and/or replicated a previous IOPs.

Campaign overview and preliminary results

The 2022 April–May SWEX campaign provided a rich environment to investigate Sundowner winds. Unprecedented datasets were collected during distinct atmospheric conditions conducive to cross-mountain downslope gusty winds. They included significant mountain waves, Sundowners during pre- and postfrontal events, and Sundowners associated with reversal critical levels (i.e., wind shear in the lower troposphere). Compound events (Sundowners during the onset of a heatwave) and conditions with weak and strong synoptic forcing (e.g., proximity of an upper-level jet, the presence of an “inside slider trough”), which, according to the NWS/LOX, have been observed in association with significant Sundowners, were also encountered during SWEX. No mission was conducted during days when a frontal system was expected to cross the region. These events complemented the SWEX pilot study (Carvalho et al. 2020) in many ways. They provided comprehensive observational measurements showing mountain waves and the lee-slope jet behavior across distinct transects of the SYM, showed spatiotemporal variability of winds and thermodynamic profiles in the ABL at unprecedented detail, and elucidated the importance of the SSMBL in the Sundowner cycle. Most importantly, SWEX created a unique database to investigate multiple meso- to turbulent-scale mechanisms associated with Sundowner evolution. This overview discusses some of the most relevant, intriguing, and promising preliminary results that will enhance the understanding of downslope winds in coastal environments.

Soon after the start of the SWEX campaign, a positive trend in temperatures marked the onset of a heatwave (Fig. 2). Models properly forecasted this event and indicated conditions for eastern Sundowners from 4–5 April (IOP-1) to 5–6 April (IOP-2). In fact, IOP-1 and IOP-2 were the first 2 days of a remarkable sequence of 5 days (5–9 April) with temperatures at RHWC1 (RAWS, SYM west slopes) and MTIC1 (RAWS, SYM east slopes) exceeding the 95th percentile of the respective spring (March–May) climatology (see Zigner et al. 2021). During IOP-1 at 2147 PDT 4 April (0447 UTC 5 April), N-NE winds on SYM eastern midslopes (MTIC1, elevation: 493 m AGL) exceeded 17 m s^{-1} and remained strong until ~ 0100 PDT 5 April. Upstream, on the mountain ridge (ISFS-11, elevation: 1,144 m AGL), wind speeds exceeded 24 m s^{-1} (Fig. 2) and exhibited similar temporal behavior as on midslope. Conversely, over western SYM near mountain ridge level (ISFS-7, 792 m AGL) and midslopes (RHWC1, 446 m AGL) in Refugio (Fig. 1) northerly winds did not exceed 10 m s^{-1} . Consistent with the expected behavior of an eastern Sundowner, wind speeds decreased from afternoon to evening over western SYM (Jones et al. 2021).

Among the most intriguing observations during IOP-1 was the presence of a mountain wave identified from CRL as a remarkable narrow layer with low water vapor mixing ratio (less than 2 g kg^{-1}) during the early evening flight (between 1842 and 1858 PDT) across eastern SYM (Fig. 3a). A narrow dry layer approximately at 800 hPa associated with a pronounced inversion layer was already evident in the first upstream dropsonde of the afternoon flight (~ 1343 PDT) at Cuyama valley (not shown). That dropsonde indicated northerly winds exceeding 20 m s^{-1} above 850 hPa on top of a deep convective ABL. Similar wind profiles were observed from the dropsonde over eastern SYV, thus consolidating favorable upstream atmospheric conditions for an eastern Sundowner (e.g., Durran 1990; Duine et al. 2021).

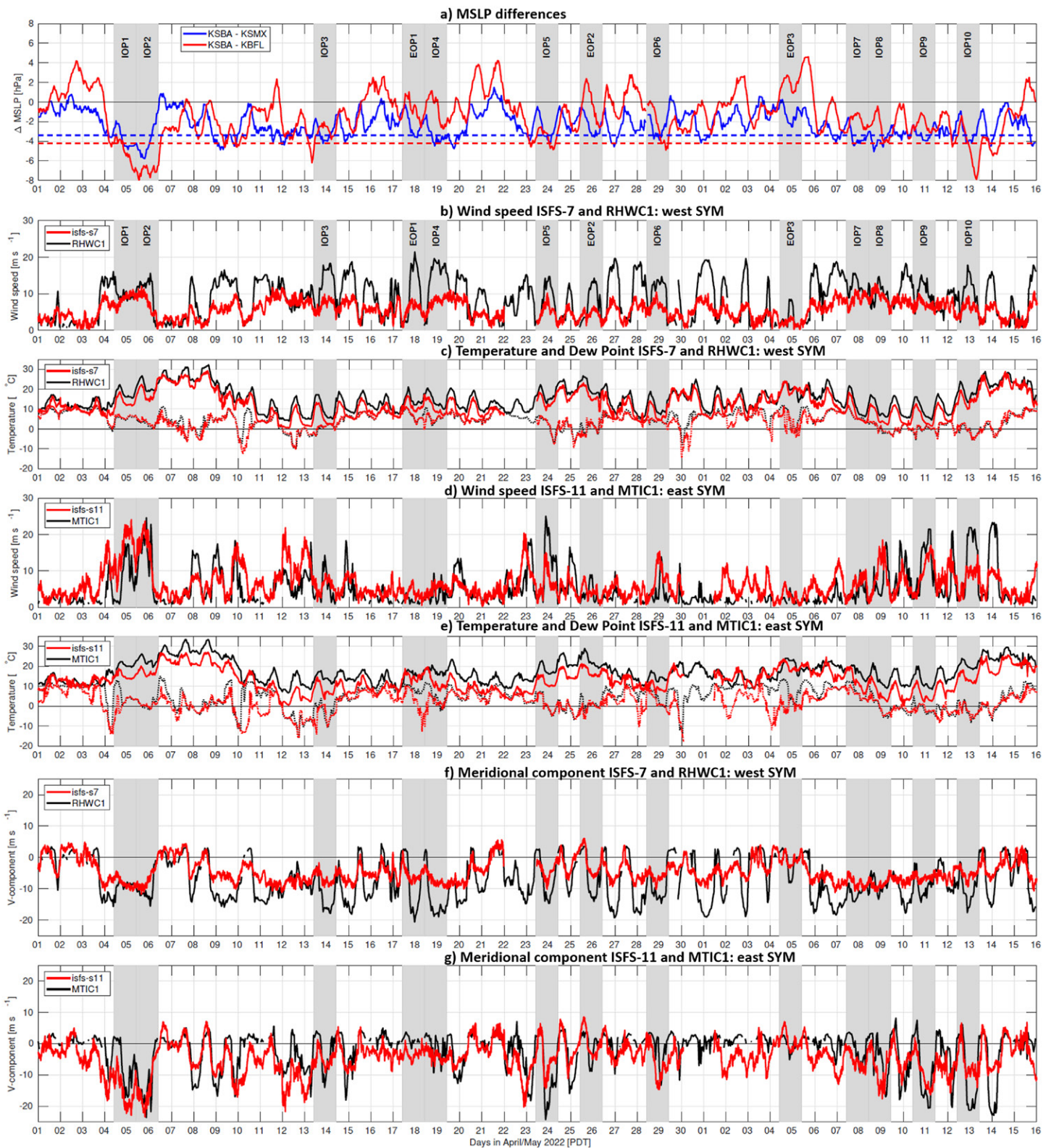


Fig. 2. (a) Time series of pressure differences between KSBA and KSMX (solid blue) and between KSBA and KFBL (solid red); (b) wind speed; (c) temperature (solid line) and dewpoint (dotted line) at ISFS-07 (black) and RHCW1 (red); (d) wind speed; (e) temperature (solid line) and dewpoint (dotted line) at ISFS-11 (black) and MTIC1 (red); (f) meridional component of the winds at ISFS-7 (red) and RHCW1 (black); (g) meridional component of the winds at ISFS-11 (black) and MTIC1 (red). IOPs and EOPs are indicated in gray. Days in April and May (horizontal axis) are labeled at 0000 PDT.

The mountain wave, with decaying amplitude away from the SYM, influenced the properties of the ABL downstream of the SYM and over the SB Channel, as shown by the airborne CRL vertical profiles of mixing ratio (Fig. 3a), aerosol distribution (Fig. 3c), and temperature (Fig. 3d).

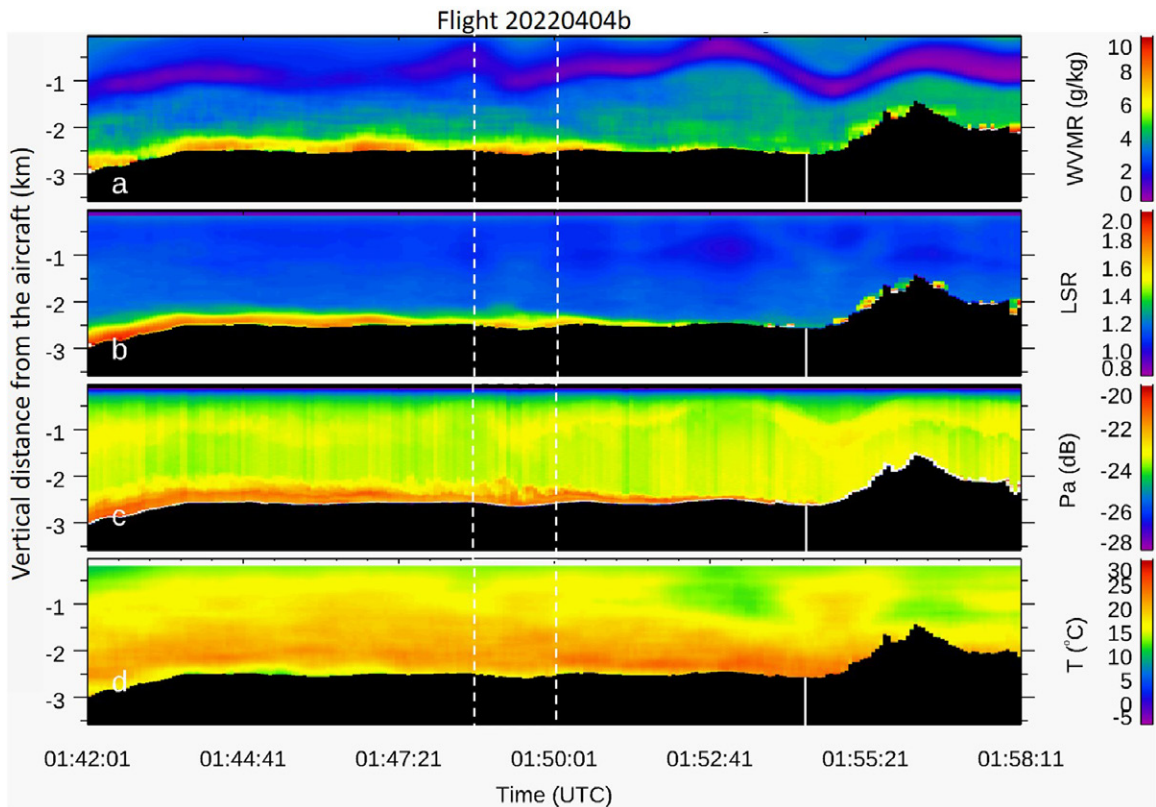


Fig. 3. CRL measurements of (a) water vapor mixing ratio, (b) aerosol lidar scattering ratio (LSR), (c) raw elastic parallel channel signals showing finer-scale aerosol distributions, and (d) temperature profiles (50-m vertical resolution, 500-m horizontal resolution) obtained across eastern SYM (track direction from south to north—see Fig. 1, track A) during IOP-1 on 4 Apr 2022. The approximate boundary between land and ocean is indicated by the vertical solid white line. Dashed white lines highlight a region with enhanced turbulent mixing, particularly evident 2 km below the aircraft (cf. measurements across the dashed lines).

The warming and cooling patterns of the lower troposphere downwind of the SYM associated with the respective wave-induced drop and rise of the isentropes are evident from the CRL temperature profile (Fig. 3c). Worth noticing is the relatively warm and dry continental ABL extending from the slopes and foothills of the eastern SYM toward the SB Channel above a shallow and cool SSMBL. Sharp horizontal and vertical contrasts between the two ABLs can be observed from the profiles of temperature, mixing ratio, and aerosols close to surface (Fig. 3), demonstrating the capability of CRL to resolve ABL processes on subkilometer scales.

The increase in turbulent mixing between the SSMBL and continental ABL (~2 km below aircraft) over the SB Channel was also noticeable from the profiles of aerosol distribution (Fig. 3c) and temperature (Fig. 3d) around 0150:01 UTC (1850:01 PDT). Note that this enhanced turbulent mixing is vertically aligned with a mountain wave trough downstream of the SYM, which is well characterized in the profile of mixing ratio (Fig. 3a). A plausible hypothesis for the enhanced turbulent mixing is the increase in vertical and horizontal wind shear (shear instability) between the two ABLs. Additional research is being conducted to investigate these mechanisms.

Temperatures and winds continued to increase over both eastern and western SYM during IOP-2 (5–6 April). North-northeasterly winds reached nearly 25 m s^{-1} (Fig. 2) approximately around 2040 PDT 5 April (0340 UTC 6 April) over eastern SYM at midslopes (MTIC1) with gusts as high as 35 m s^{-1} (the highest gusts registered at that site during the SWEX campaign, not shown). Winds with similar magnitudes and direction were observed at mountain ridge (ISFS-11). Among the unique aspects of IOP-2 was the remarkable difference in mean sea level

pressure (MSLP) between the KSBA and KBFL airports (~ -8 hPa), which has been frequently associated with strong eastern Sundowners (Sukup 2013). Similar MSLP differences during the SWEX campaign were observed only in IOP-10 (Fig. 2). Moreover, large MSLP differences between KSBA and KSMX airports (-5 hPa), which indicates potential for western Sundowners, were also observed during IOP2. Consistent with this, N-NW winds exceeding 15 m s^{-1} were recorded at RHWC1 (western SYM) after midnight (local time), indicating that this was a “hybrid” regime (Fig. 2).

The SJSU Doppler lidar on the foothills of the westernmost site in Gaviota (Fig. 1) revealed in detail important features associated with the Sundowner evolution over western SYM during IOP-2 (Fig. 4). Northerly winds exceeding 15 m s^{-1} were present late afternoon (\sim at 1700 PDT) at approximately 500 m AGL. These winds progressively intensified and turned northwestward as they approached ground level. The lee-slope jet appeared well characterized between 1900 and 2100 PDT in the lidar profile (Fig. 4a). Concomitantly, northerly (cross-mountain) winds increased to 10 m s^{-1} at ISFS-12 (elevation: 766 m), which is located on the western SYM near Gaviota peak, upstream of the lidar site (Fig. 1). The association between Sundowners and the lee-slope jet has been hypothesized before based on models (e.g., Duine et al. 2019; Smith et al. 2018) and radiosonde observations during the pilot study (Carvalho et al. 2020). IOP-2 allowed a detailed characterization of the lee-slope jet behavior.

The SJSU Doppler lidar documented two other important features: the intermittency of the lee-slope jet and the transition of wind direction from N-NW before 2100 PDT to N-NE after 2100 PDT (albeit with weaker magnitudes). The N-NE winds nearly coincided with the maximum N-NE winds observed over eastern SYM at MTIC1 and ISFS-11 (Fig. 2). The peak of cross-mountain winds at ISFS-12 was observed between 2200 and 2330 PDT (Fig. 4b) preceding a sharp increase in temperature (Fig. 4c) of about 5°C on the foothills (ISFS-1). Dewpoint temperature also dropped approximately the same amount, but more gradually at ISFS-1 after the onset of the northerly winds.

Another remarkable feature of IOP-2 was an abrupt demise of the lee-slope jet after 0200 PDT 6 April, when the N-NE winds with magnitudes exceeding 10 m s^{-1} transitioned to weak winds (less than 2 m s^{-1}) in a layer extending from the surface up to 1,000 m AGL, with predominantly easterly direction above 500 m AGL (Fig. 4a). In tandem, dewpoint increased $\sim 8^\circ\text{C}$ whereas temperature decreased $\sim 9^\circ\text{C}$ at foothills (ISFS-1), contrasting with the nearly constant values at higher elevations (ISFS-12). These observations suggest a clear intrusion of a shallow marine ABL and its importance in the Sundowner cycle (Malarkey 2023).

IOP3 (13–14 April) was a typical western Sundowner, with strong (weak) winds over western (eastern) SYM. It provided an opportunity to investigate cross-mountain winds 3 days after the passage of a frontal system but within a period with below-seasonal-average temperatures and dewpoints (Fig. 2). UWOW captured well the contrasts of wind profiles and the remarkable transition of wind regimes along the east–west-oriented U.S. 101 (Fig. 5a). Noticeable are the westward decrease in elevation and increase in intensity of the NW lee-slope jet (Fig. 5b), which characterizes the western Sundowners (cf. Figs. 5c–e). Another intriguing feature of these profiles is the presence of “double lee-slope jets” (Fig. 5d), indicating the importance of turbulent mixing in the deepening of the lee-jet toward lower elevations, which may explain the spatial and temporal variability of near ground level winds. At the surface, JSU-MMU observed alternating bands of dry and moist air on the slopes and foothills of western SYM under descending Sundowners (Fig. 6). Note that the sharp drop in dewpoint of more than 2°C around 300 m MSL seems consistent with the enhancement of the lee-slope jet shown with UWOW between longitudes 120.05 and 120.01 (Fig. 5b).

An important SWEX goal was to characterize spatial contrasts in winds and temperature profiles and identify their dependence on Sundowner regimes. IOP-4 (18–19 April) gathered observations during a western Sundowner in prefrontal conditions and was associated with

SJSU Doppler Lidar, Gaviota

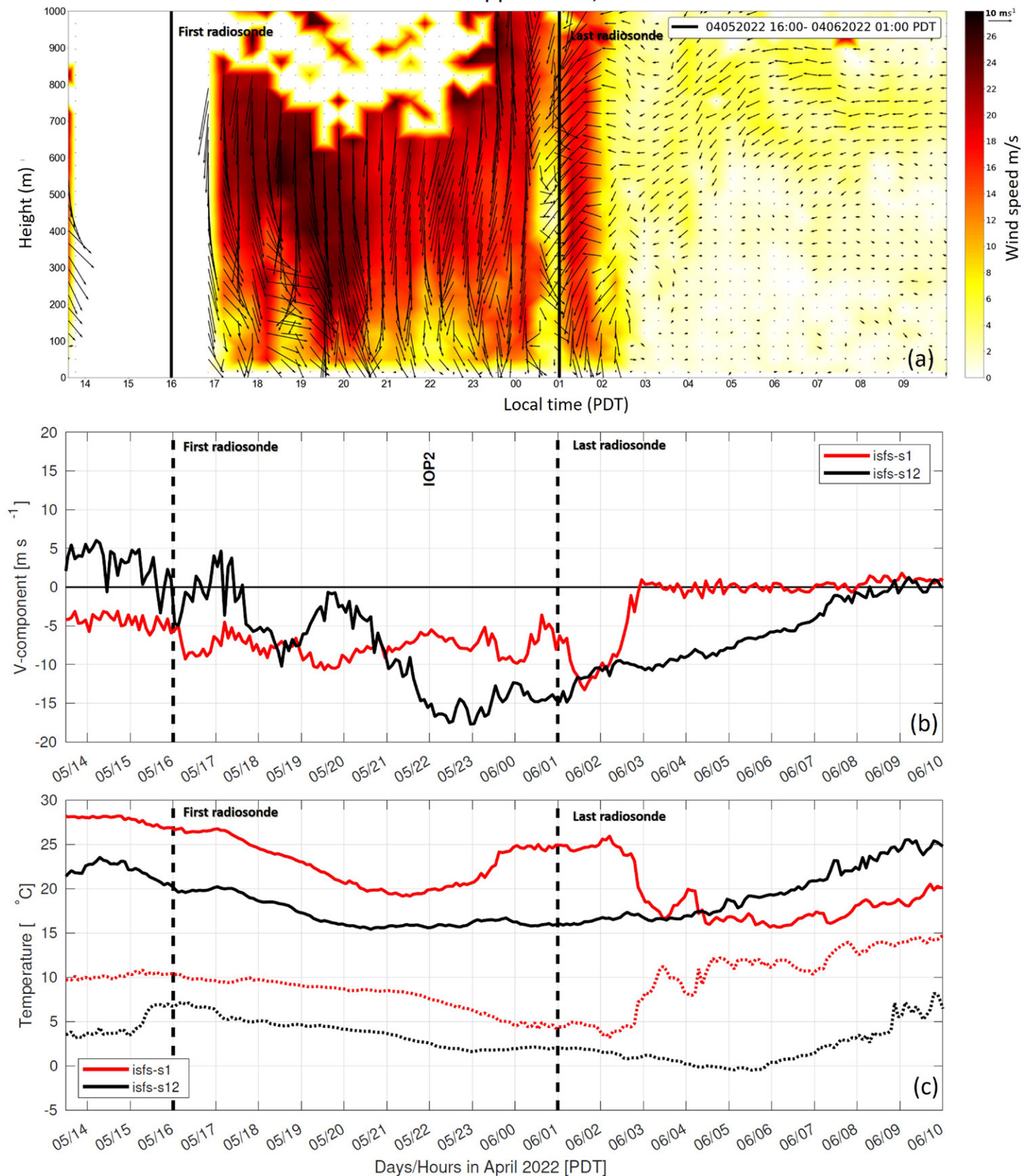


Fig. 4. (a) SJSU Doppler lidar wind profile obtained over the western foothills of the SYM (GVT, Fig. 1) from ~1400 PDT 5 Apr to 1000 PDT 6 Apr during IOP-2. Colors indicate wind speed (m s^{-1}) and quivers represent wind speed and direction. Missing data from 1400 to 1700 PDT 4 Apr 2022 were caused by power outage. (b) Time series of observed 10-m winds (meridional component) at ISFS-1 (Gaviota foothills, elevation: 65.37m MSL) and ISFS-12 (Gaviota mountains, elevation: 766.13m MSL). (c) 2-m temperatures (solid lines) and dewpoint (dotted lines) for ISFS-1 (red) and ISFS-12 (black). Vertical lines indicate the first and last radiosonde during IOP-2 (from Malarkey 2023).

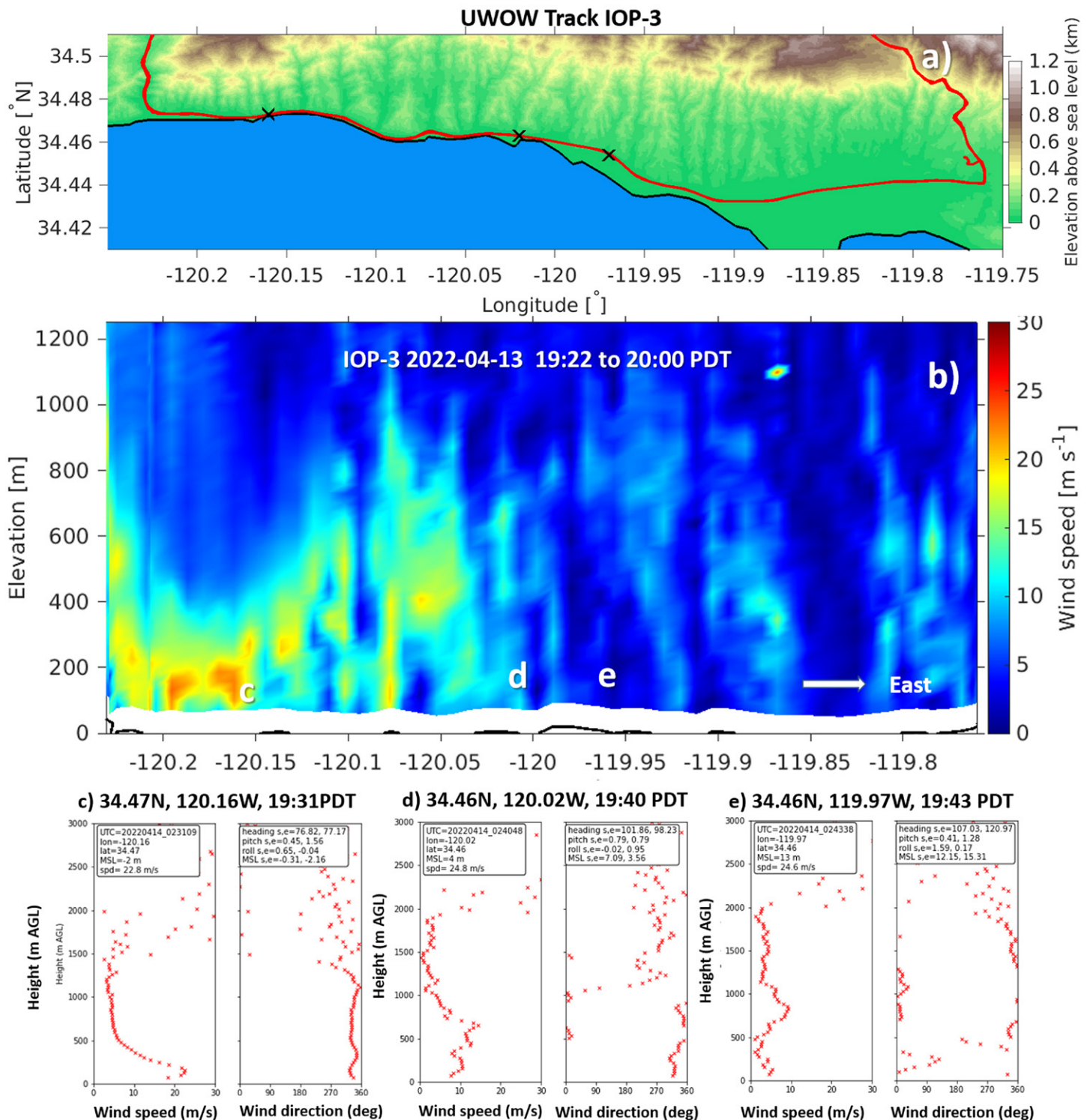


Fig. 5. UWOW wind profiles during IOP-3. (a) East–west-oriented U.S. 101 where profiles were collected (indicated by the x symbols); (b) UWOW integrated ABL wind profiles obtained along the U.S. 101; (c)–(e) profiles of (left) wind speed and (right) wind direction at three distinct sites on the U.S. 101 obtained during early evening hours on 13 Apr (coordinates and time PDT are indicated at the top of each frame).

an approaching trough and directional wind shear in the lower troposphere. Consistent with a western Sundowner, winds reaching 20 m s^{-1} were observed on the western SYM mid slopes (RHWC1) while light winds (less than 10 m s^{-1}) were observed at mid slopes of eastern SYM (MCIT1) during the evening (Fig. 2).

Figure 7 shows airborne CRL temperature profiles across eastern SYM at different periods during IOP-4 evening flight (1807–2200 PDT). The temperature structure clearly contrasted

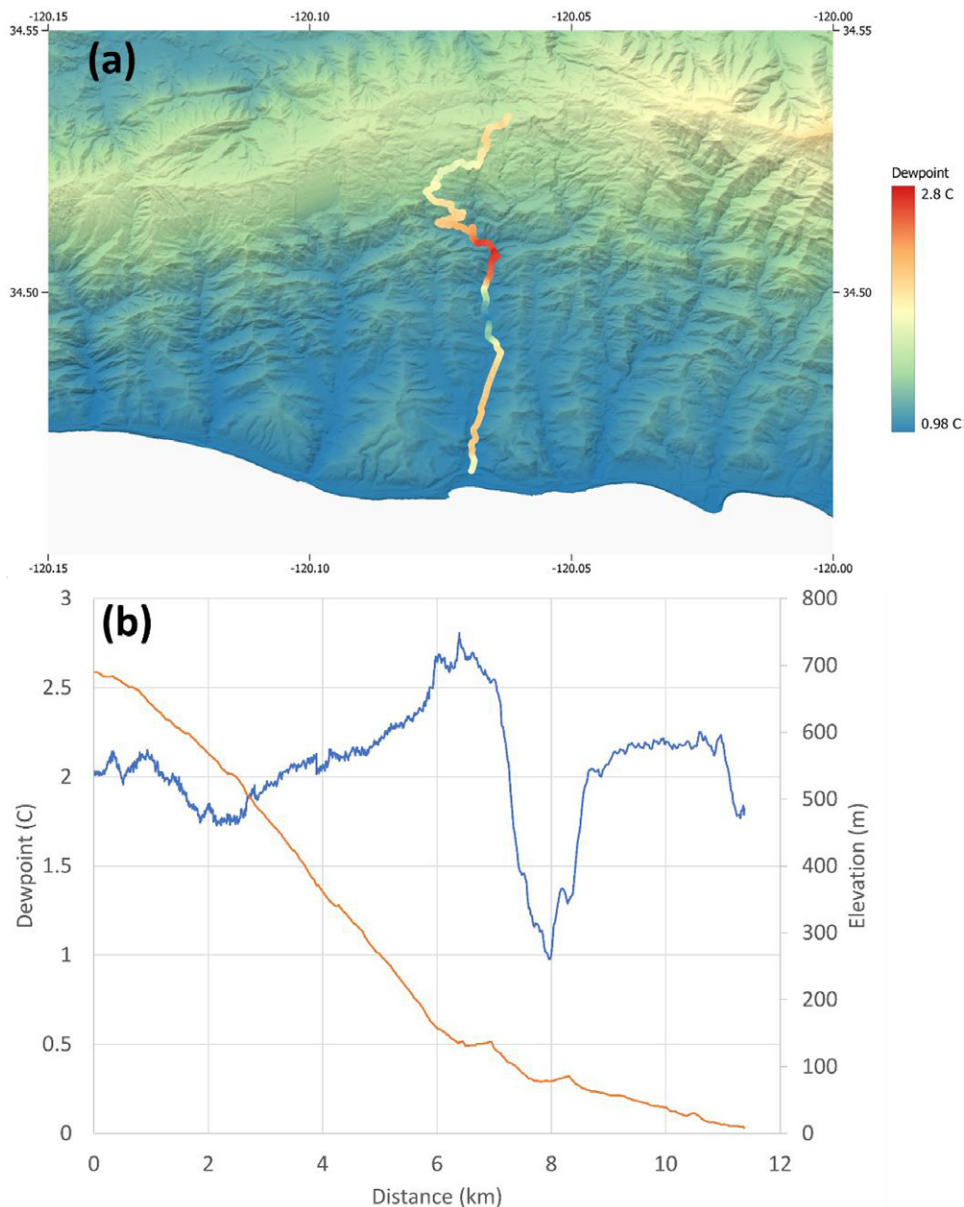


Fig. 6. (a) JSU-MMU dewpoint temperature measurements descending from Refugio Pass to Refugio Beach during IOP-3 between 2046 and 2118 PDT 13 Apr (0346–0418 UTC 14 Apr). The nearly north–south line at the center of the figure shows the driven road and colors on that path indicate the observed dewpoint temperature (see color bar). The background map shows the local terrain (arbitrary shading, with lighter colors representing higher elevations) (b) JSU-MMU simultaneous elevation (red line) and dewpoint temperature (blue line) during the descending track shown in (a).

with the oscillatory pattern observed when mountain waves were present during IOP-1 (cf. Fig. 7 with Fig. 4d). A multilayered temperature structure was observed downstream of the SYM extending above the SB Channel in the late afternoon (Fig. 7a, 1807–1812 PDT). All SB Channel dropsondes confirmed the presence of two distinguishable inversion layers below 800 hPa, both characterized by a sharp decrease in mixing ratio (not shown). While WSW winds exceeding 20 m s^{-1} were systematically observed above 700 hPa, evening dropsondes indicated that wind speeds varied significantly over the channel at lower altitudes, with winds weakening eastward. Above the eastern SB Channel, the 2152 PDT 18 April dropsonde (0452 UTC 19 April) showed predominantly WNW light winds (less than 5 m s^{-1}) between 800 and 1,000 hPa. Interestingly, CRL indicated the presence of a well-defined warm layer, with thickness of about 1 km downstream of the SYM extending above the cool and shallow SSMBL from 1800 PDT (Fig. 7a) to 2018 PDT (Fig. 7b), with the warmest profiles observed

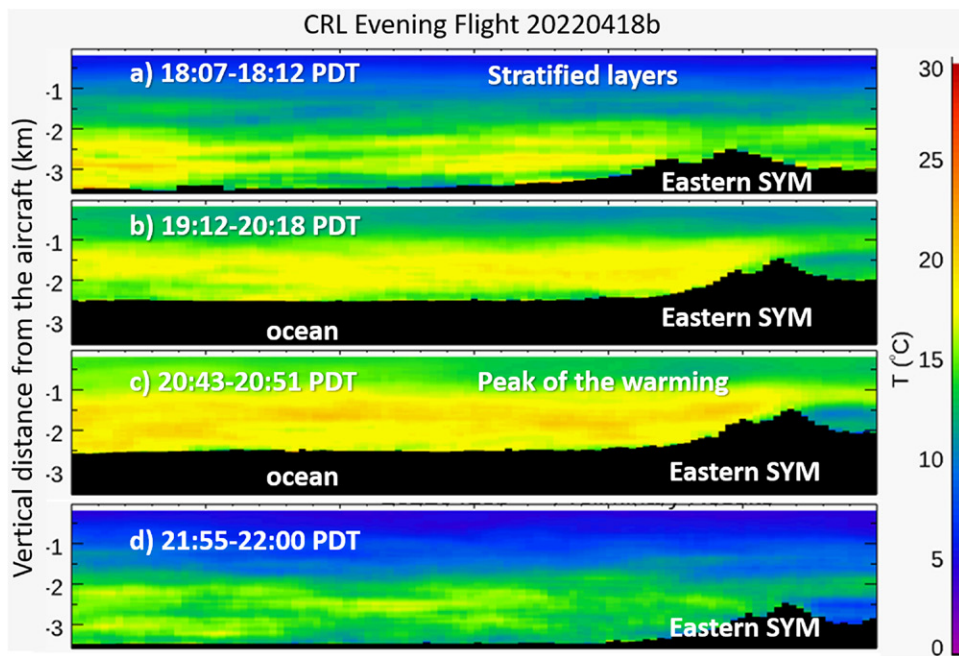


Fig. 7. CRL temperature obtained on 18 April evening flight across eastern SYM during IOP-4. Time period (PDT) of the flight track is indicated in each frame. Note that the horizontal and vertical axes differ in each frame, as they depend on the flight duration and elevation of the aircraft relative to the surface, respectively.

over the channel during the 2043–2051 PDT flight (Fig. 7c). Note how temperature contrasts downstream and upstream of the SYM increased from 1800 to 2100 PDT, with warmer (cooler) profiles observed above the SB Channel (SYV) during all flights. These contrasts led to a strong temperature gradient next to the SYM top ridge. This temperature gradient and the layered-temperature structure over the SB channel were shown for the first time with a suite of instrument platforms. Further analyses are necessary to understand physical and dynamical processes explaining these features and relationships with winds and stability profiles.

Another hybrid Sundowner was observed on 23–24 April (IOP-5) with synoptic conditions favoring low relative humidity (Fig. 2). We use IOP-5 to examine the performance of HRRR and WRF (v4.2.2) in forecasting a lee-slope jet across eastern SYM and the sensitivity of these forecasts to resolution and land surface model (LSM) parameterizations. Figures 8a and 8b show south–north cross sections of wind speed (shaded) and potential temperature (contoured) across Montecito valid at 0400 UTC 24 April extracted from the HRRR operational runs commencing at 1200 UTC 23 and 0000 UTC 24 April, respectively. This time corresponded with the fastest northerly winds (24.3 m s^{-1}) observed at MTIC1 during the campaign (Fig. 2). HRRR forecasted a downslope flow accelerating as it passed over the tallest peak in the SRM (labeled “A” in Fig. 8a), and progressing across the SYV (“B”), and over and down the SYM across Montecito (“C”).

WRF simulations (finest grid spacing: 667 m), selected from an extensive physics ensemble and initialized with the HRRR (Fig. 8a), produced stronger downslope flow across Montecito, partly due to the better resolution of the narrow SYM. Airflow characteristics farther inland and offshore, however, differed among these simulations and from HRRR. WRF configured comparably to the HRRR (Fig. 8c) shows downslope flow executing a high-amplitude hydraulic jump on the lee of the SYM with some lee wave activity (“E”). The strong winds did not extend all the way to the coastline at this time, and the SSMBL could still be seen offshore. Farther inland, the fast SRM lee-side flow elevated across the SYV, resulting in lighter wind conditions near the ground there (“F”). The Pleim–Xiu LSM scheme (Fig. 8d) led to a smaller-amplitude jump (“G”) without lee waves. Flow across the SYV (“H”)

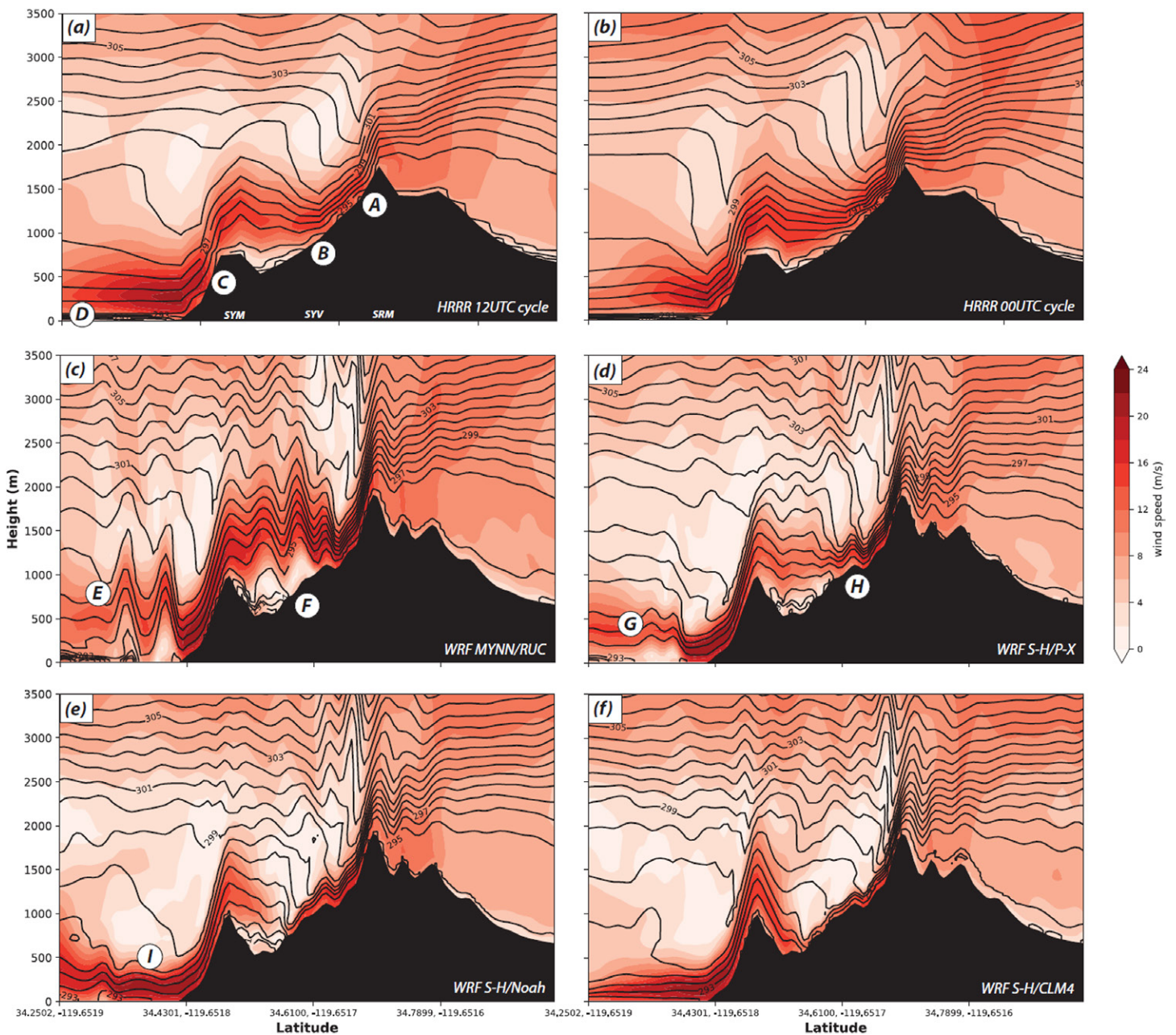


Fig. 8. South–north vertical cross sections across Montecito of wind speed (shaded) and potential temperature (1-K contours) valid at 0400 UTC (2100 PDT) 24 Apr (IOP-5), representing (a) the HRRR 1200 UTC 23 Apr 16-h forecast and (b) the HRRR 0000 UTC 24 Apr 4-h forecast. (c)–(f) The 16-h forecasts from WRF (grid spacing: 667 m) physics ensemble members using (c) MYNN PBL (Olson et al. 2019) and surface layer and RUC LSM (Smirnova et al. 2016), and Shin–Hong PBL (Shin and Hong 2015) and revised MM5 surface layer (Jimenez et al. 2012) with LSMs (d) Pleim–Xiu (Pleim 2006), (e) Noah (Tewari et al. 2004), and (f) CLM4 (Lu and Kueppers 2012). White circles labeled with capital letters (A–I) are explained in the text. Note that the two HRRR simulations initialized 12 h apart in (a) and (b) look very similar and in both the downslope winds lofted prior to reaching the coastline, leaving the shallow and stable marine layer (“D”) intact over the coastal plain.

was also less elevated in this run. With the Noah LSM (Fig. 8e), the strong winds flowed much closer to the surface (“I”) and pushed the SSMBL farther out to sea. That tendency was even more exaggerated when the CLM4 LSM was used (Fig. 8f). The Noah and CLM4 LSMs presumed the lowest land surface roughness in the area, while RUC and Noah-MP (not shown) were among the highest; this factor has shown to be important with downslope winds (Cao and Fovell 2016, 2018; Duine et al. 2019). Note the differences upwind of the SRM were much subtler. These examples illustrate the complexity in forecasting downslope windstorms in coastal mountains and the importance of SWEX in providing comprehensive datasets to properly investigate modeling performance.

Accurately forecasting whether strong winds will “surface” in an environment where ABLs with different properties interact on multiple scales is challenging but recognizably impactful to properly issuing red-flag warnings and planning public safety power shutoffs (PSPS IOP-6, 28–29 April) was among the most intriguing IOPs to evaluate Sundowner overprediction for many reasons. Forecasts consistently indicated that a generalized windstorm associated with a postfrontal system should affect most of the SYM southern slopes during the IOP, similarly to the “Santa Barbara” Sundowners identified in Jones et al. (2021). While winds intensified during nighttime, observations showed that models overestimated near-ground magnitudes over both eastern and western SYM (Fig. 2). UWOW wind profiles indicated dramatic changes in the intensity and elevation of the lee-slope jet during this IOP (Fig. 9a), suggesting enhanced turbulence above 500 m AGL. WRF forecast (2-km resolution) misrepresented this variability, forecasting strong winds below 500 m (Fig. 9b). Interestingly, aircraft measurements and the SJSU lidar in Gaviota (not shown) indicated a very turbulent atmosphere. CRL profiles of temperature across Refugio (Fig. 9c) showed the presence of gravity waves mostly confined to layers above 2–3 km, which were clearly misrepresented by WRF 2-km forecast (Fig. 9d). Relationships between the elevated turbulence and the weakening of the surface winds are presently unknown.

The SWEX campaign was supposed to end with IOP-9, if it was not for an opportunity that could not be missed on 12–13 May (IOP-10): investigate an eastern/hybrid Sundowner associated with weak synoptic forcing (weak upper-level support) but with a forecast of KSBA–KBFL MSLP differences exceeding the 99.9th percentile. Another unique aspect of this event was the consistent agreement between GFS and ECMWF in forecasting these features for more than 7 consecutive days, which was unusual during SWEX. The NWS/LOX rely primarily

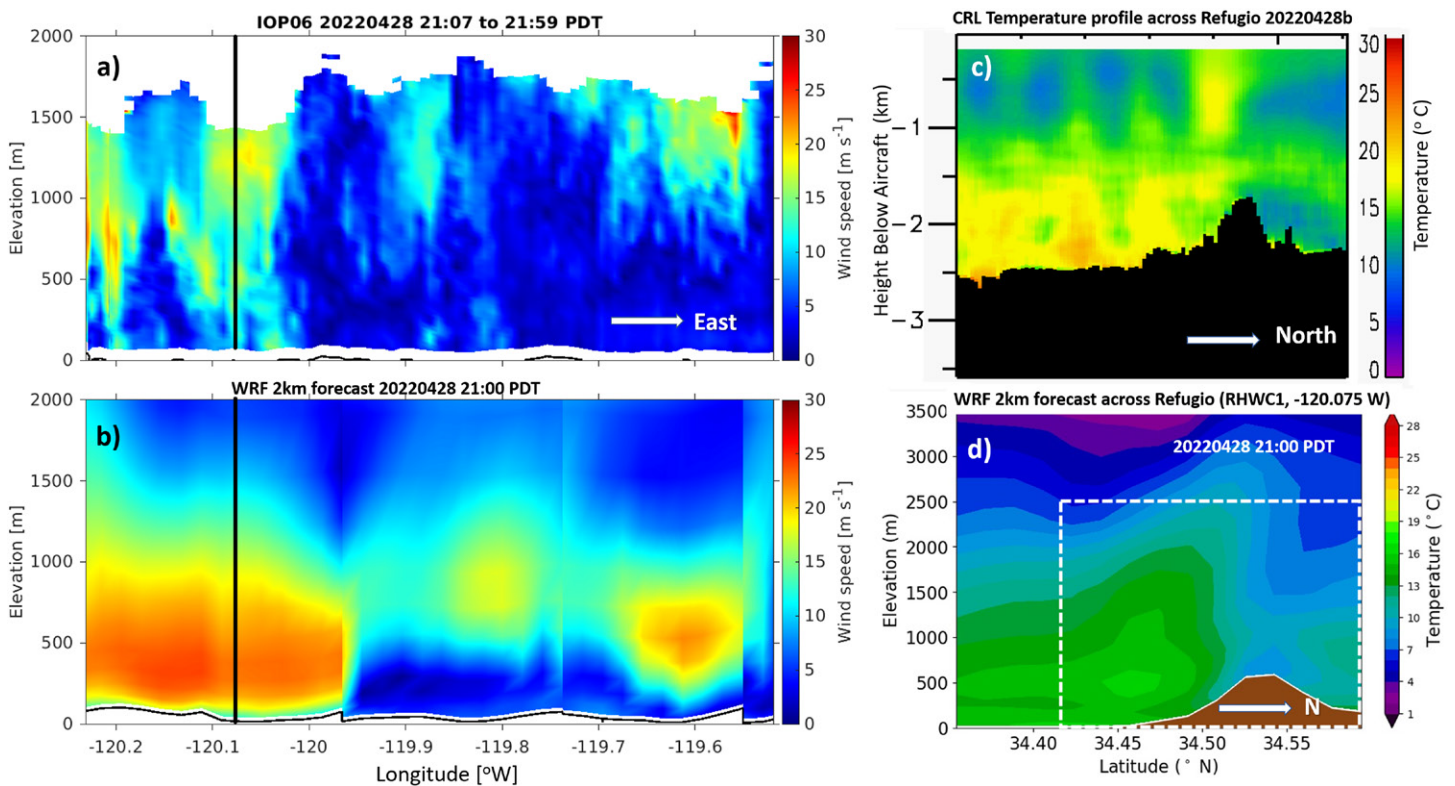


Fig. 9. (a) UWOW wind profiles obtained along the U.S. 101 during IOP-6 between 2107 and 2159 PDT 28 Apr; (b) WRF hourly forecast (2-km grid spacing) temporally interpolated during the period of data collected by UWOW (reason for the apparent discontinuity of the profiles at some longitudes); (c) Twin-Otter CRL profile of temperature across Refugio along the longitude indicated by the thick black vertical line in (a); (d) WRF forecast (2-km grid spacing) of temperature profiles at 2100 PDT along the same longitude. The area enclosed by the white dashed lines covers approximately the same domain as the CRL cross section in (c). WRF configuration in (b) and (c) is as in Jones et al. (2021).

on these forecasts, and the interest in this event had practical implications for operational forecasting. However, except for a few radiosondes sufficient for two sites during a half-day mission, few resources were left for IOP-10, and those excluded the Twin-Otter flight hours. Since IOP-10 was supposed to be a hybrid Sundowner with stronger winds expected east of the SYM in Montecito, UWOW was maintained stationary at the Montecito Fire Department station 2 (MFS-2; Fig. 1). This site (151 m MSL elevation) approximately aligns (north–south direction) with MTIC1 and ISFS-11 (Fig. 1).

Figure 10 illustrates IOP-10 by showing the temporal variability of horizontal wind speed and vertical velocity profiles from three lidars on the eastern SYM foothills (from east to west): NCAR/EOL at the SBCFD-HQ, UND at the SB Botanic Garden (BOT), and UWOW at MFS-2 (Fig. 1). The onset of Sundowners at SBCFD-HQ (wind speeds exceeding 10 m s^{-1}) was quite abrupt near sunset (around 1800 PDT) and was associated with descending vertical motion between about $3\text{--}4 \text{ m s}^{-1}$, indicating the strengthening of the lee-slope jet from mountaintop to foothills. However, close to ground level winds nearly ceased by 2100 PDT at that location. East, at BOT and MFS-2, winds exhibited temporal oscillations that were remarkably similar despite their distance (these sites are $\sim 5 \text{ km}$ apart in an east–west direction), and stronger wind magnitudes at MFS-2. NE winds exceeding 20 m s^{-1} (with gusts exceeding 30 m s^{-1}) were observed at MCIT1 (Fig. 2), consistent with the horizontal wind profiles at MFS-2.

Vertical velocities were also similar between BOT and MFS-2 (Fig. 10), with ascending magnitudes reaching $+6 \text{ m s}^{-1}$ in both sites coinciding with the lifting of the strongest winds to about 1,000 m AGL (approximately mountaintop elevation). The similarity between the two profiles and the strong updrafts with comparable magnitudes suggest that both sites were influenced by a mountain wave with similar horizontal and vertical structure, and both were affected by the wave’s hydraulic jump. This is supported by CRL observations of the mountain wave across Montecito during the eastern Sundowner in IOP-1 (Fig. 3). UWOW observations indicated increased eddy dissipation rates during periods with strong updrafts (not shown), explaining decaying winds near ground level. Similar mechanisms may have played a role in the weakening and reintensification of the lee-slope jet during the SWEX pilot study (Carvalho et al. 2020). The strongest winds at MFS-2 and MTIC1 were observed between 0100 and 0400 PDT 13 May, whereas the KSBA–KBFL MSLP differences were the largest around 0700 PDT 13 May, demonstrating the importance of mountain waves and the hydraulic jump in the behavior of near-ground winds and their forecast. A detailed analysis of IOP-10, including conditions upstream, is being conducted to further explore these results.

SWEX unique and challenging aspects

The landscape and rough topography of the SYM and SRM imposed challenges to the SWEX instrument design, particularly concerning the placement of flux towers. For example, some critical and remote sites at mountain ridgeline and mountain slopes were only accessible using unpaved and narrow roads and trails, complicating efforts for installation and maintenance of the instruments. Finding a perfect fetch, undisturbed by trees and not significantly influenced by the presence of canyons and gorges that could affect the representativeness of the measurements, were among the greatest difficulties of the campaign design. Moreover, the presence of trees and distribution power lines occasionally limited the ability to uninterruptedly observe winds using the UWOW on roads along the SYM slopes. Despite these challenges, SWEX collected rich datasets showing significant variability of Sundowner winds and the environment they occur.

Sundowner is a phenomenon with most of the “action” happening from early evening of one day until early morning of the next day. The 3-hourly radiosondes (from 1000 to 0700 PDT), as well as the late evening flights and ground mobile operations, represented a major challenge for the SWEX team during the campaign. Thanks to the professionalism and commitment

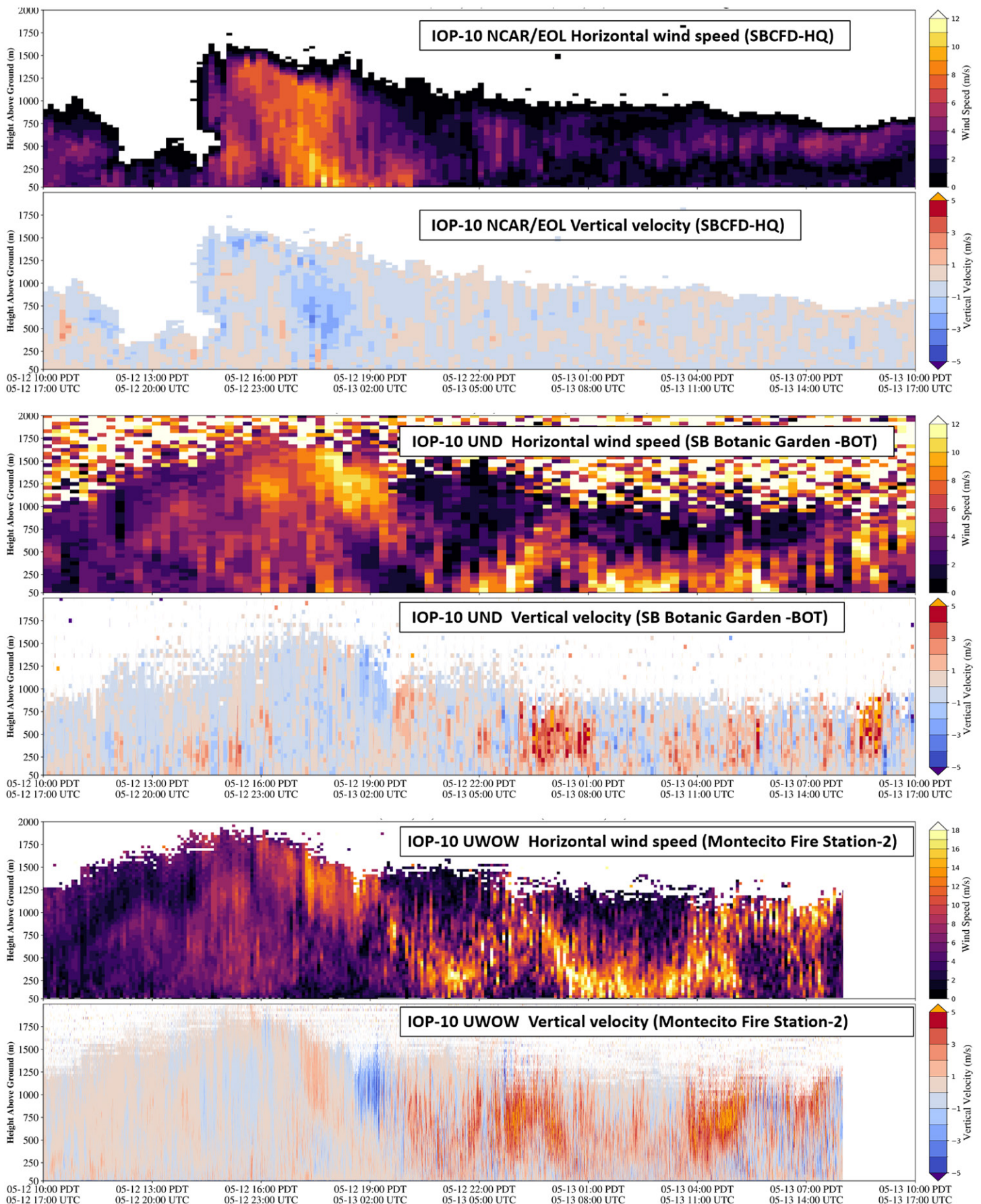


Fig. 10. Temporal variability of horizontal wind speed and vertical velocity profiles observed by three stationary lidars during IOP-10. Lidar location is indicated at the top of each panel (see Fig. 1). Note that, for the sake of clarity and a proper comparison among profiles, the range of magnitudes of horizontal winds for UWOW is larger. From de Orla-Barile (2023).

of graduate and undergraduate students and postdocs, the NPS pilots and staff, and the exceptional coordination of the SWEX team, all missions were successfully accomplished.

While the broad spectrum of cross-mountain wind conditions was a desirable outcome of the 2022 SWEX campaign, it imposed challenges to decide upon IOPs and EOPs representative of both the unique and most common conditions observed during Sundowners within the 45 days of the campaign. Although no IOP completely disappointed concerning the nighttime onset of gusty winds over western and/or eastern slopes of the SYM, some events were overpredicted (e.g., IOP-6), whereas other potential events were underestimated (Fig. 2). These events and particularly IOP-6 provide opportunities to evaluate important reasons for numerical forecast errors.

Among the SWEX campaign's fortuitous observing periods were the 4–5 and 5–6 April compound events, when consecutive days with eastern Sundowners occurred along with the onset of a heatwave (IOPs 1 and 2). Eastern Sundowners are not as common as western Sundowners (Jones et al. 2021); neither are heatwaves in spring. Moreover, Sundowners observed during hot and dry days significantly increase the risk of fast-spreading wildfires (Zigner et al. 2022). Thus, the opportunity to investigate a rare event added value to the SWEX campaign and provided rich observations to contrast with the summer compound event (Sundowner during a heatwave) discussed in Duine et al. (2022).

A surprising aspect of the SWEX campaign was the short lasting and relatively weak winds throughout the night at the central-eastern site (SBCFD-HQ) during most IOPs, which contrasted with the SWEX pilot study (Carvalho et al. 2020). This aspect has triggered new investigations focusing on physical and dynamical processes conducive to the intrusion of the SSMBL.

The SWEX campaign was delayed two years due to the COVID-19 pandemic but was successfully completed in 2022 without any incidents thanks to excellent cooperation and coordination of all the involved parties.

Summary and outlook

This overview synthesizes 13 missions (10 IOPs and 3 EOPs) during the 2022 SWEX campaign and highlights some of the most interesting contributions of novel observing systems to advance understanding of downslope windstorms in coastal mountains influenced by contrasting ABLs. Unique and rich datasets obtained from sophisticated multiplatform instrumentation were collected during 45 days (1 April–15 May), and new measurement strategies were successfully tested during special missions. While comprehensive research to unveil mechanisms and evaluate modeling performance and predictability of Sundowner winds is underway, SWEX preliminary results have already illustrated the potential for innovative theories on downslope windstorms and their mechanisms. Sundowners have unique and common features with other windstorms worldwide. SWEX observations will build new pillars for future concepts and novel research on mountain meteorology for years to come.

SWEX preliminary analyses have already shown relevant and promising results that will guide future investigations. A stratified atmosphere and temperature contrasts across the SYM and over the SB Channel have been remarkable features identified by airborne measurements. Mountain waves were observed associated with strong Sundowner winds, extending their influence downstream of the SYM and above the SB Channel. The lee-slope jet has properties and characteristics that significantly vary spatially and temporally. The onset of Sundowners seemed related to the intensification and extension of the lee-slope jet from mountaintop to lower elevations, which appeared controlled by turbulent processes and mountain wave characteristics. Lidars indicated sharp transitions in wind speeds and direction and remarkable differences in wind profiles along the east–west-oriented SYM foothills that depend on

Sundowner wind regimes. SWEX demonstrated the role of the marine ABL in the demise of the downslope winds and how transitions from gusty to calm winds near the surface can be abrupt in time and space.

Stationary and airborne lidars confirmed that mountain waves exhibit mesoscale features that control wind behavior on regional scales, as suggested in the SWEX pilot experiment (Carvalho et al. 2020). In some locations where lidars observed hydraulic jumps, ascending air reached speeds as high as 6 m s^{-1} , which nearly exceeded 25% of the observed maximum horizontal winds magnitudes during an event. These are regions with enhanced turbulent eddy dissipation that act to significantly alter the intensity and elevation of the lee-slope jet, and thus wind speeds and gusts next to ground level. All these features are difficult to simulate using operational regional models, even at subkilometer grid resolution. Preliminary modeling studies showed great sensitivity of WRF simulations to LSM and PBL schemes. SWEX observational datasets will be invaluable in conducting new numerical experiments to improve model configurations aiming at realistically representing downslope winds in coastal environments.

Sundowner mechanisms are complex and SWEX preliminary results evidenced the importance of understanding physical and dynamical processes interacting on multiple spatiotemporal scales. The broad spectrum of atmospheric conditions associated with cross-mountain winds and flow acceleration on the southern slopes of the SYM collected during SWEX demonstrated that a proper characterization of Sundowner winds, their mechanisms, and relationships with other known types of downslope winds require further research. Additional studies focusing on the structure and contrasts between the SSMBL and continental ABL, and respective interactions with western and eastern Sundowners are of primary importance. The influence of mean-state critical levels and upstream stability effects on mountain wave characteristics and mechanisms, and consequent impacts on Sundowner magnitudes and predictability, need a detailed examination. Sundowners are influenced by flow interactions from two east–west-oriented mountain ranges, with decreasing distance and increasing elevation from west to east. The effect of the SRM on mountain waves and downstream impact on downslope flow acceleration on the SRM and SYM have yet to be understood. The SWEX integrated multiplatform observations are invaluable assets to investigate these and other issues, and ultimately improve forecast and advance new theories on downslope winds in coastal mountains.

The SWEX campaign had significant broad impacts. For example, SWEX provided unique opportunities for 23 undergraduate and graduate students from five campuses (UCSB, SJSU, UND, CU, UAlbany) to learn about the state-of-art instrumental platforms collecting ABL datasets while experiencing the dynamics and significance of teamwork coordination during a field campaign (Fig. 11). Making accurate Sundowner forecasts is a great priority for the NWS/LOX. The SWEX campaign strengthened existing collaborations between scientists and the NWS/LOX, effectively bridging research interests to operational forecast needs. This collaboration will continue flourishing as new research is developed.

Given the recognized role of Sundowners in fast-spreading wildfires toward populated areas of SB, SWEX was greatly appreciated by local communities living in the SB coast and SYV, attracting the interest of the local media and residents of all ages (Fig. 11). SWEX students and scientists attended numerous public panels and presented seminars during the campaign, communicating the importance of the novel datasets and scientific studies to residents, fire fighters, and local decision-makers.

The campaign received invaluable logistic support from the SB County Fire Department, Montecito Fire Department, and the U.S. Forest Service. The benefits of this synergy are many and perhaps best exemplified by the engagement between SWEX scientists, fire marshals, and fire fighters. SWEX missions created opportunities to exchange experiences and discuss



Fig. 11. Examples of the educational and outreach components of the SWEX campaign. (left) Graduate students being trained by NCAR staff on radiosonde launching at the Sedgwick Reserve; (right) Boy Scout Camporee event held at the Rancho Alegre site during the SWEX campaign attended by 150 scouts from across the region. NCAR staff gave a talk and tour of the ISS site and launched a sounding with an enthusiastic group of scouts.

the importance of the campaign to understand and predict the most critical fire weather affecting the wildfire prone communities in SB County.

Acknowledgments. The professionalism and commitment of forecasters of the NWS/LOX during the 45 days of the SWEX campaign and during the campaign design phase are much appreciated. Their diligent participation in mission decision was invaluable for the success of SWEX.

We acknowledge the logistic support of the SB County Fire Department (SBCFD), Montecito Fire Department (MFD), and the U.S. Forest Service (USFS). In particular, we thank Chief Rob Hazard (SBCFD) for working along with the SWEX team from pre- to postdeployment, helping in selecting sites and actively participating in numerous discussions concerning campaign goals and safety of all individuals. The SBCFD and MFD kindly offered their facilities to shelter the SWEX team day and night while providing safe places to install critical instruments.

The attention, guidance, and encouragement kindly offered by Dr. Vanda Grubisic and Brigitte Baeuerle from conception to realization of the SWEX campaign were critical and much appreciated.

We heartily thank the NSF program managers for working with the team to overcome the obstacles imposed by the COVID pandemic.

EOL Carol Constanza is much appreciated for her dedication to the field catalogue, and Jacquie Witte and Matthew Paulus, EOL associate scientists, for the QC work on both ISS and ISFS. We acknowledge the exceptional work of EOL engineering, software, and technical teams, and professionalism of EOL ISFS and ISS teams that faced numerous challenges to place, maintain, and dismantle numerous instruments in the rough terrain of SB County in 2020 and 2022.

The dedication and competence of the Twin-Otter pilots and all those involved in flight operation are much appreciated.

We recognize the commitment and professionalism of 23 graduate and undergraduate students that tirelessly conducted radiosonde launches during day and night without fail, often under harsh meteorological conditions. We thank the logistic support of staff and volunteers at the UCSB Sedgwick Reserve.

We express our gratitude to the following individuals for offering logistic support to the campaign: Rob Hazard, Bob Hazard, Steve Kiss, Jay Ruskie, Patrice A. Surmeier, Das Williams, among others.

We thank the anonymous reviewers and Dr. Maria Silva Dias for their enthusiasm and thoughtful comments for the improvement of this manuscript.

This material is based upon work supported by the National Center for Atmospheric Research, which is a major facility sponsored by the National Science Foundation (NSF) under Cooperative Agreement 1852977.

This research has been supported by the following grants: NSF AGS-1921595 (Carvalho, Duine, Fitzjarrald, Jones, White), NSF AGS-1921596 (Wang), NSF AGS-1921554 (Fernando), NSF AGS-1921546 (Fovell), NSF AGS-1921583 (Clements), NSF AGS-1921504 (De Wekker), University of California Office of the President Laboratory Fees Programs LFR-20652467 (Seto, Thompson), Gordon and Betty Moore Foundation 11601 (Duine).

The Naval Postgraduate School CIRPAS Twin Otter research aircraft operations and measurements (Bucholtz, Emmitt, and Greco) were funded by NSF under Interagency Agreement IAA21392160001. Additional Twin Otter flight hours and airborne Doppler Wind Lidar wind profiles were funded by supplemental funding from the Office of Naval Research Document N0001421PR00501.

Data availability statement. The field catalog with daily reports, mission summary, and data access can be obtained at the SWEX field catalog <http://catalog.eol.ucar.edu/swex>.

The SWEX Data Archive and field catalog was built and maintained by NCAR/EOL.

Appendix A: List of acronyms and abbreviations

AVAPS	Airborne Vertical Atmospheric Profiling System dropsonde
ABL	Atmospheric boundary layer
BOT	Santa Barbara Botanic Garden (UND site)
CIRPAS	Center for Interdisciplinary Remotely Piloted Aircraft Studies
CRL	Compact rotational Raman lidar
CU	University of Colorado Boulder
ECMWF	European Centre for Medium-Range Weather Forecasts
EOL	NCAR Earth Observing Laboratory
EOP	Extended operation period
GFS	Global Forecast System
GVT	Gaviota (ISFS, SJSU, UAlbany site)
HP	Hazard Property (ISFS, UND site)
HQ	Santa Barbara County Fire Department Headquarters (ISS, UCSB site)
HRRR	High-Resolution Rapid Refresh
IOP	Intensive operation period
ISFS	Integrated Surface Flux System
ISS	Integrated Sounding System
JSU	Jackson State University
JSU-MMU	Jackson State University, Mobile Meteorological Unit
KBFL	Bakersfield Airport
KIZA	Santa Ynez Airport/Kunkle Unit (UND site)
KOXX	Oxnard Airport
KSBA	Santa Barbara Airport
lidar	Light detection and ranging
LSM	Land surface model
ONR	Office of Naval Research
MFS-2	Montecito Fire Department, Station 2
MSLP	Mean sea level pressure
NAM	North American Mesoscale Forecast System
NCAR	National Center for Atmospheric Research
NCEP	National Centers for Environmental Prediction
NPS	Naval Postgraduate School
NWS	National Weather Service
NWS/LOX	National Weather Service, LA–Oxnard office
RA	Rancho Alegre (ISS site)

RASS	Radio Acoustic Sounding System
RAWS	Remote Automatic Weather Station
SB	Santa Barbara
SBCFD-HQ	Santa Barbara County Fire Department Headquarters
SBCFD-38	Santa Barbara County Fire Department Station 38
SDG	Sedgwick Reserve (ISS, ISFS site)
SJSU	San Jose State University
SRM	San Rafael Mountains
SSMBL	Stably stratified marine boundary layer
SYM	Santa Ynez Mountains
SYV	Santa Ynez valley
TODWL	Twin-Otter Doppler Wind Lidar
UAlbany	University at Albany, State University of New York
UCSB	University of California, Santa Barbara
UND	University of Notre Dame
USFS	U.S. Forest Service
UVA	University of Virginia
UWOW	University of Virginia Wind Observatory on Wheels
UWy	University of Wyoming
WCL	Wyoming Cloud Lidar
WRF	Weather Research and Forecasting Model

Appendix B: Overview of instruments

Table B1 provides an overview of the instruments used in this study.

Table B1. Instruments, focus, location (site, latitude, longitude, and elevation), instrument provider, and operating period during SWEX. For a list of acronyms, see appendix A.

Instrument	Focus	Location [site, lat (°N), lon (°W), elevation (m)]	Institution	Operation period
Stationary lidars				
Doppler lidar (Halo photonics)	Downstream, west SYM	Gaviota SBFD-38, 34.47694, 120.21432, 74.05	SJSU	1 Apr–11 May
Doppler lidar	Downstream central-east SYM	SBFD-HQ, 34.4516, 119.7694, 85.75	NCAR EOL	1 Apr–15 May
Doppler lidar	Downstream, west SYM	Refugio (HP), 34.5186111, 120.0791666, 474.84	UND	1 Apr–15 May
Doppler lidar	Downstream east SYM	SB Botanic Garden (BOT), 34.45508, 119.70871, 221.87	UND	1 Apr–15 May
Doppler lidar	Upstream SYV	KIZA, 34.606, 120.077, 205.0	UND	1 Apr–15 May
Doppler lidar (UWOW)	Downstream east SYM	Montecito Fire Station 2 (MFS2), 34.44021, 119.65934, 146.79	UVA	12–13 May
Wind profilers				
449 MHz (ISS1)	Downstream, central-east SYM	SBCFD-HQ, 34.4527, 119.7712, 91.02	NCAR EOL	1 Apr–15 May
915 MHz (ISS2)	Upstream, central SYV	Rancho Alegre (RA), 34.56306, 119.95028, 374.9	NCAR EOL	1 Apr–15 May
915 MHz (ISS3)	Upstream, northwest SYV	Sedgwick Reserve (SDG), 34.6874, 120.0384, 340.69	NCAR EOL	1 Apr–15 May
Ceilometers				
Vaisala CL31 (ISS1)	Downstream, central-east SYM	SBCFD-HQ, 34.4527, 119.7712, 91.02	NCAR EOL	1 Apr–15 May
Vaisala CL51 (ISS2)	Upstream, central SYV	Rancho Alegre (RA), 34.56306, 119.95028, 374.9	NCAR EOL	1 Apr–15 May
Vaisala CL31 (ISS3)	Upstream, northwest SYV	Sedgwick Reserve (SDG), 34.6874, 120.0384, 340.69	NCAR EOL	1 Apr–15 May
Vaisala CT25K	Downstream west SYM	Gaviota–SBFD-38, 34.47679, 120.21432, 74.05	UAlbany	1 Apr–15 May
Vaisala CL31	Downstream, west SYM	Refugio (HP), 34.5186111, 120.0791666, 474.84	UND	1 Apr–15 May
Vaisala CL31	Upstream SYV	KIZA, 34.606, 120.077, 205.0	UND	1 Apr–15 May
Vaisala CL31	Downstream east SYM	SB Botanic Garden (BOT), 34.45508, 119.70871, 221.87	UND	1 Apr–15 May

(Continued)

Table B1. (Continued).

Instrument	Focus	Location [site, lat (°N), lon (°W), elevation (m)]	Institution	Operation period
Various				
Infrasound unit 1	Downstream west SYM	Gaviota–SBCFD-38, 34.47647, 120.21459, 71.33	UAlbany	1 Apr–11 May
Infrasound unit 2	Downstream west SYM	Gaviota–SBCFD-38, 34.47584, 120.21544, 67.10	UAlbany	1 Apr–11 May
Infrasound unit 2	Downstream west SYM	Gaviota–SBCFD-38, 34.4758, 120.21389, 62.82	UAlbany	1 Apr–11 May
Microwave radiometer	Upstream SYV	KIZA, 34.606, 120.077, 205.0	UND	1 Apr–15 May
Radiosondes				
Vaisala (ISS2)	Upstream, central SYV	Rancho Alegre (RA), 34.56306, 119.95028, 374.9	NCAR EOL	IOPs and EOPs
Vaisala (ISS3)	Upstream, northwest SYV	UCSB Sedgwick Reserve (SDG), 34.6874, 120.0384, 340.69	NCAR EOL	IOPs and EOPs
GRAW 1	Downstream west SYM	Gaviota, SBCFD-38, 34.4765, 120.21447, 74.05	SJSU	IOPs and EOPs
GRAW 2	Downstream, central-east SB	SBCFD-HQ, 34.4509, 119.7694, 81.28	SJSU/UCSB	IOPs and EOPs
Surface sensors				
ISFS flux tower 1	Downstream west SYM	Gaviota, 34.4758272, 120.2146195, 65.37	NCAR EOL	1 Apr–15 May
ISFS flux tower 2	Downstream west SYM	Goleta, 34.475615, 119.920130, 224.27	NCAR EOL	1 Apr–15 May
ISFS flux tower 3	Downstream west SYM	El Capitan Canyon, 34.465763, 120.027416, 56.19	NCAR EOL	1 Apr–15 May
ISFS flux tower 4	Downstream east SYM	San Marcos Preserve, 34.45924, 119.7643, 143.85	NCAR EOL	1 Apr–15 May
ISFS flux tower 5	Downstream, west SYM	Refugio, 34.48284, 120.05044, 204.37	NCAR EOL	1 Apr–15 May
ISFS flux tower 6	Downstream, west SYM	Refugio, 34.5190340, 120.0789333, 481.31	NCAR EOL	1 Apr–15 May
ISFS flux tower 7	West SYM ridgeline	Bald Mountain, 34.5302339, 120.0927446, 791.57	NCAR EOL	1 Apr–15 May
ISFS flux tower 8	Central SYM ridgeline	Santa Ynez Peak, 34.5303416, 119.9875286, 1235.69	NCAR EOL	1 Apr–15 May
ISFS flux tower 9	East SYM ridgeline	Knapp’s Castle, 34.520205, 119.785680, 1010.39	NCAR EOL	1 Apr–15 May
ISFS flux tower 10	East SYM ridgeline	La Cumbre Peak, 34.500530, 119.722015, 1199.68	NCAR EOL	1 Apr–15 May
ISFS flux tower 11	East SYM ridgeline	Montecito, 34.4893769, 119.6499334, 1144.0	NCAR EOL	1 Apr–15 May
ISFS Flux tower-12	West SYM ridgeline	Gaviota Peak, 34.5059778, 120.1899385, 766.13	NCAR EOL	1 Apr–15 May
ISFS flux tower 13	Upstream, central SYV	Rancho Alegre (RA), 34.55756, 119.94080, 374.9	NCAR EOL	1 Apr–15 May
ISFS flux tower 14	Upstream, NW SYV	UCSB Sedgwick Reserve (SDG), 34.6955305, 120.0471357, 373.75	NCAR EOL	1 Apr–15 May
ISFS flux tower 15	Upstream SRM	Figueroa Mountain, 34.731979, 120.010007, 972.24	NCAR EOL	1 Apr–15 May
ISFS flux tower 16	Upstream upper SYV	Little Pine Mountain, 34.599367, 119.747283, 1356.52	NCAR EOL	1 Apr–15 May
ISFS flux tower 17	Upstream Cuyama	Cuyama Peak, 34.754246, 119.477299, 1396.44	NCAR EOL	1 Apr–15 May
ISFS flux tower 18	Downstream central east	San Marcos Pass, 34.494511, 119.824009, 620.78	NCAR EOL	1 Apr–15 May
Met tower	Upstream west SYV	KIZA, 34.606, 120.077, 205.0	UND	1 Apr–15 May
Met tower	Downstream west SYM	Refugio, 34.519, 120.079, 474.84	UND	1 Apr–15 May
RAWS MCT1	Downstream east SYM	Montecito, 34.461, 119.649, 493.4712	USFS	Permanent
RAWS RHWC1	Downstream west SYM	Refugio, 34.517, 120.075, 446.532	USFS	Permanent
Mobile platforms, instruments, spatial coverage, instrument provider, and operation period				
Mobile-JSU MMU	Temperature, dewpoint temperature, pressure, brightness temperature	SYV, SYM ridgeline and southern slopes	JSU	IOPs and EOPs
Doppler lidar (UWOW)	Vertical wind profiles	SYV, SYM slopes and foothills	UVA	IOPs and EOPs
Doppler lidar (TODWL)	Vertical wind profiles	Twin-Otter tracks (Fig. 1)	ONR	IOPs and EOPs
Raman lidar	Temperature, humidity, aerosol profiles	Twin-Otter tracks (Fig. 1)	CU	IOPs and EOPs
Cloud lidar	Cloud microphysics and optical parameters	Twin-Otter tracks (Fig. 1)	UWy	IOPs and EOPs

References

- Blier, W., 1998: The Sundowner winds of Santa Barbara, California. *Wea. Forecasting*, **13**, 702–716, [https://doi.org/10.1175/1520-0434\(1998\)013<0702:TSWOSB>2.0.CO;2](https://doi.org/10.1175/1520-0434(1998)013<0702:TSWOSB>2.0.CO;2).
- Cannon, F., L. M. V. Carvalho, C. Jones, T. Hall, D. Gombert, J. Dumas, and M. Jackson, 2017: WRF simulation of downslope wind events in coastal Santa Barbara County. *Atmos. Res.*, **191**, 57–73, <https://doi.org/10.1016/j.atmosres.2017.03.010>.
- Cao, Y., and R. G. Fovell, 2016: Downslope windstorms of San Diego County. Part I: A case study. *Mon. Wea. Rev.*, **144**, 529–552, <https://doi.org/10.1175/MWR-D-15-0147.1>.
- , and —, 2018: Downslope windstorms of San Diego County. Part II: Physics ensemble analyses and gust forecasting. *Wea. Forecasting*, **33**, 539–559, <https://doi.org/10.1175/WAF-D-17-0177.1>.
- Carvalho, L. M. V., and Coauthors, 2020: The Sundowner Winds Experiment (SWEX) pilot study: Understanding downslope windstorms in the Santa Ynez Mountains, Santa Barbara, California. *Mon. Wea. Rev.*, **148**, 1519–1539, <https://doi.org/10.1175/MWR-D-19-0207.1>.
- de Orla-Barile, M., 2023: A case study from the Sundowner Wind Experiment: Intensive operation period #10 (May 12–13, 2022). M.S. thesis, Dept. of Geography, University of California, Santa Barbara, 46 pp.
- De Wekker, S. F. J., K. S. Godwin, and G. D. Emmitt, 2012: Airborne Doppler lidar measurements of valley flows in complex coastal terrain. *J. Appl. Meteor. Climatol.*, **51**, 1558–1574, <https://doi.org/10.1175/JAMC-D-10-05034.1>.
- Duine, G.-J., C. Jones, L. M. V. Carvalho, and R. G. Fovell, 2019: Simulating Sundowner winds in coastal Santa Barbara: Model validation and sensitivity. *Atmosphere*, **10**, 155, <https://doi.org/10.3390/atmos10030155>.
- , L. M. V. Carvalho, C. Jones, and K. Zigner, 2021: The effect of upstream topography on the onset of Sundowner winds in coastal Santa Barbara, CA. *J. Geophys. Res. Atmos.*, **126**, e2020JD033791, <https://doi.org/10.1029/2020JD033791>.
- , —, and —, 2022: Mesoscale patterns associated with two distinct heatwave events in coastal Santa Barbara, California, and their impact on local fire risk conditions. *Wea. Climate Extremes*, **37**, 100482, <https://doi.org/10.1016/j.wace.2022.100482>.
- Durrant, D. R., 1990: Mountain waves and downslope winds. *Atmospheric Processes over Complex Terrain*, Meteor. Monogr., Vol. 23, Amer. Meteor. Soc., 59–81, https://doi.org/10.1007/978-1-935704-25-6_4.
- Emmitt, G. D., and K. Godwin, 2014: Advanced airborne Doppler wind lidar signal processing for observations in complex terrain. *Proc. SPIE*, **9246**, 924609, <https://doi.org/10.1117/12.2068226>.
- Hatchett, B. J., C. M. Smith, N. J. Nauslar, and M. L. Kaplan, 2018: Synoptic-scale differences between Sundowner and Santa Ana wind regimes in the Santa Ynez Mountains, California. *Nat. Hazards Earth Syst. Sci.*, **18**, 419–427, <https://doi.org/10.5194/nhess-18-419-2018>.
- Jimenez, P. A., J. Dudhia, J. F. Gonzalez-Rouco, J. Navarro, J. P. Montavez, and E. Garcia-Bustamante, 2012: A revised scheme for the WRF surface layer formulation. *Mon. Wea. Rev.*, **140**, 898–918, <https://doi.org/10.1175/MWR-D-11-00056.1>.
- Jones, C., L. M. V. Carvalho, G.-J. Duine, and K. Zigner, 2021: Climatology of Sundowner winds in coastal Santa Barbara, California, based on 30-yr high resolution WRF downscaling. *Atmos. Res.*, **249**, 105305, <https://doi.org/10.1016/j.atmosres.2020.105305>.
- Liu, B., Z. Wang, Y. Cai, P. Wechsler, W. Kuestner, M. Burkhart, and W. Welch, 2014: Compact airborne Raman lidar for profiling aerosol, water vapor and clouds. *Opt. Express*, **22**, 20613–20621, <https://doi.org/10.1364/OE.22.020613>.
- Lu, Y., and L. M. Kueppers, 2012: Surface energy partitioning over four dominant vegetation types across the United States in a coupled regional climate model (Weather Research and Forecasting Model 3–Community Land Model 3.5). *J. Geophys. Res.*, **117**, D06111, <https://doi.org/10.1029/2011JD016991>.
- Malarkey, K., 2023: Sundowners and mountain wave activity: Selected observations from the Sundowner Winds Experiment (SWEX). M.S. thesis, Dept. of Meteorology and Climate Science, San Jose State University, 72 pp.
- Olson, J. B., J. S. Kenyon, W. Angevine, J. M. Brown, M. Pagowski, and K. Sušelj, 2019: A description of the MYNN-EDMF scheme and the coupling to other components in WRF–ARW. NOAA Tech. Memo. OAR GSD-61, 42 pp., <https://doi.org/10.25923/n9wm-be49>.
- Pleim, J. E., 2006: A simple, efficient solution of flux–profile relationships in the atmospheric surface layer. *J. Appl. Meteor. Climatol.*, **45**, 341–347, <https://doi.org/10.1175/JAM2339.1>.
- Rahn, D. A., T. R. Parish, and D. Leon, 2013: Airborne measurements of coastal jet transition around Point Conception, California. *Mon. Wea. Rev.*, **141**, 3827–3839, <https://doi.org/10.1175/MWR-D-13-00030.1>.
- Ryan, G., 1996: Downslope winds of Santa Barbara, California. NOAA Tech. Memo. NWS WR 240, 44 pp., <https://repository.library.noaa.gov/view/noaa/14746>.
- Shin, H. H., and S. Y. Hong, 2015: Representation of the subgrid-scale turbulent transport in convective boundary layers at gray-zone resolutions. *Mon. Wea. Rev.*, **143**, 250–271, <https://doi.org/10.1175/MWR-D-14-00116.1>.
- Skamarock, W. C., and Coauthors, 2019: A description of the Advanced Research WRF Model version 4. NCAR Tech. Note NCAR/TN-556+STR, 145 pp., <https://doi.org/10.5065/1dfh-6p97>.
- Smirnova, T. G., J. M. Brown, and S. G. Benjamin, 2016: Modifications to the Rapid Update Cycle Land Surface Model (RUC LSM) available in the Weather Research and Forecasting (WRF) Model. *Mon. Wea. Rev.*, **144**, 1851–1865, <https://doi.org/10.1175/MWR-D-15-0198.1>.
- Smith, C., B. Hatchett, and M. Kaplan, 2018: Characteristics of Sundowner winds near Santa Barbara, CA, from a dynamically downscaled climatology: Environment and effects aloft and offshore. *J. Geophys. Res. Atmos.*, **123**, 13 092–13 110, <https://doi.org/10.1029/2018JD029065>.
- Sukup, S., 2013: Extreme northeasterly wind events in the hills above Montecito, California. NWS Western Region Tech. Rep. NWS WR-1302, 21 pp., www.weather.gov/media/wrh/online_publications/talite/talite1302.pdf.
- Tewari, M., and Coauthors, 2004: Implementation and verification of the unified Noah land surface model in the WRF Model. *20th Conf. on Weather Analysis and Forecasting/16th Conf. on Numerical Weather Prediction*, Seattle, WA, Amer. Meteor. Soc., 14.2a, https://ams.confex.com/ams/84Annual/techprogram/paper_69061.htm.
- Vömel, H., and Coauthors, 2021: High-resolution in situ observations of atmospheric thermodynamics using dropsondes during the Organization of Tropical East Pacific Convection (OTREC) field campaign. *Earth Syst. Sci. Data*, **13**, 1107–1117, <https://doi.org/10.5194/essd-13-1107-2021>.
- Wang, Z., P. Wechsler, W. Kuestner, J. French, A. Rodi, B. Glover, M. Burkhart, and D. Lukens, 2009: Wyoming Cloud Lidar: Instrument description and applications. *Opt. Express*, **17**, 13 576–13 587, <https://doi.org/10.1364/OE.17.013576>.
- White, L. D., 2014: Mobile observations of a quasi-frontal transient moisture boundary in the Deep South. *Wea. Forecasting*, **29**, 1356–1373, <https://doi.org/10.1175/WAF-D-14-00009.1>.
- , and D. Lu, 2020: Multi-scale transects of three North American drylines. *Atmosphere*, **11**, 854, <https://doi.org/10.3390/atmos11080854>.
- Wu, D., and Coauthors, 2016: Airborne compact rotational Raman lidar for temperature measurement. *Opt. Express*, **24**, A1210–A1223, <https://doi.org/10.1364/OE.24.0A1210>.
- Zigner, K., L. M. V. Carvalho, S. Peterson, F. Fujioka, G.-J. Duine, C. Jones, D. Roberts, and M. Moritz, 2020: Evaluating the ability of FARSITE to simulate wildfires influenced by extreme, downslope winds in Santa Barbara, California. *Fire*, **3**, 29, <https://doi.org/10.3390/fire3030029>.
- , —, C. Jones, and G.-J. Duine, 2021: Extreme winds and fire weather in coastal Santa Barbara County, CA: An observational analysis. *Int. J. Climatol.*, **42**, 597–618, <https://doi.org/10.1002/joc.7262>.
- , and Coauthors, 2022: Wildfire risk in the complex terrain of the Santa Barbara wildland-urban interface during extreme winds. *Fire*, **5**, 138, <https://doi.org/10.3390/fire5050138>.